Electronic Supplementary Material (ESI) for Reaction Chemistry & Engineering.

Supporting Information

Guided Optimization of a Crystallization-Induced Diastereomer Transformation to Access a Key Navoximod Intermediate

Andrew J. Kukor,[a] Frédéric St-Jean,[b] Andy Stumpf,[b] Thomas C. Malig,[c] Katarzyna A. Piechowicz,[b] Kenji Kurita,[c] and Jason E. Hein[a]*

[a] Department of Chemistry, The University of British Columbia, Vancouver, BC V6T 1Z1, Canada

[b] Department of Small Molecule Process Chemistry, Genentech, Inc., South San Francisco, California, 94080, United States

[c] Department of Small Molecule Analytical Chemistry Quality Control, Genentech, Inc., South San Francisco, California, 94080, United States

*email for J.E.H.: jhein@chem.ubc.ca

Table of Contents

1. General Info

a. Chemical Suppliers

L-Dibenzoyl tartaric acid (L-DBTA) monohydrate and HPLC grade acetonitrile were purchased from Sigma. Optima-grade HPLC solvents, 4-acetamidophenol, potassium carbonate (K_2CO_3) and sodium bicarbonate ($NaHCO_3$) were purchased from Fisher. Racemic 2-(6-fluoro-5H-imidazo[5,1-a]isoindol-5-yl)-1-((1r,4r)-4-hydroxycyclohexyl)ethan-1-one (*rac*-**1**) was supplied by Genentech, Inc. All other reagents and solvents were purchased from conventional suppliers and used as received unless otherwise stated.

b. Equipment Setup

All experiments were performed in Mettler-Toledo EasyMax 102 Advanced Thermostat System glass reactors (50 mL, 100 mL or 250 mL) equipped with Teflon reactor/port covers, submersible thermocouple, and a magnetic stir bar controlled by the Mettler-Toledo software iControl 6.1. The internal reactor temperature (T_r) was maintained by the EasyMax and measured by a thermocouple placed directly inside the reactor. Inline racemization made use of an EasyMax thermostat unit, a VapourTec SF-10 reagent pump, and a custom-made inline racemization chamber connected via the minimum amount of IDEX ETFE 1/8" OD x 1/16" ID tubing. The inline racemization chamber was designed to have tubing coiled around it while fitting inside an EasyMax 102 reactor well (see section SI 2b). A disposable ETFE filter was added to the tubing drawing solution out of the reactor (*i.e.,* the line leading to the pump inlet) to ensure that only the solution phase was passed through the inline racemization chamber.

Mettler-Toledo's iC Vision software was used in conjunction with a Mettler-Toledo EasyViewer probe for the acquisition of turbidity data and crystal images. A Bruker D8-Advance X-ray diffractometer was used to obtain powder x-ray diffraction (PXRD) data. Temporal concentration data was obtained using a custom-built automation rig comprised of an EasySampler, diluent solvent pump, combined 6-port valve, solenoid valve and pressure sensor module (CombiValve) and an Agilent 1290 Infinity HPLC connected in series. A custom-built filter tip attachment was used to facilitate solution-phase exclusive sampling with the EasySampler.[1] Control of all components except the HPLC was carried out by a custom in-house built control module (DI Box) capable of triggering the EasySampler extension and retraction, pump operation and speed, valve positions, monitoring inline pressure, and sending a signal to trigger the collection of HPLC data. This DI Box controls all components necessary for direct injection of samples from the EasySampler onto the HPLC and is operated by means of a custom-built Python script and graphic user interface. Agilent's Chemstation program was used in conjunction with our DI Box to acquire and analyze samples as frequently as sample run times would allow. Sampling events were controlled via third party software sending a signal at the requested sampling frequency (*e.g.*, every 15 minutes) to our Python script, which would then carry out the necessary functions required to obtain a sample and transport it via diluent solvent to the HPLC. A normal sampling sequence with the running Python script looks like:

1. Third party software sends the signal to our Python script that it is time to begin the sampling sequence
2. The EasySampler is extended
3. The pump is started and pre-fills the lines with a specified volume of diluent solvent at a specified flow rate
4. The EasySampler is retracted

5. The 6-port valve position is changed such that the sample loop is now inline with the pump and EasySampler
6. The pump is started and pushes the sample through the lines into the inline sample loop on the 6-port valve
7. The 6-port valve position is changed such that the sample loop is now inline with the HPLC
8. A signal is sent from the DI Box to the HPLC (Chemstation) to begin data collection
9. The pump is started and the lines are washed with a specified volume of diluent solvent
10. The solenoid valve is actuated and an alternate solvent is selected
11. The pump is started and the lines are filled with the alternate solvent (such that extension of the EasySampler introduces 20 µL of this solvent and not diluent into the reaction)
12. The solenoid valve is actuated and returned to the diluent solvent position for the next sampling sequence
13. The third party software waits for a signal from Chemstation that the current HPLC run is over before sending the signal to begin the next run

Offline HPLC samples were acquired using a Microlit RBO 1000 µL micropipette, delivered into a Corning Costar Spin-X 0.45 µm Nylon centrifuge tube filter in a 2.0 mL polypropylene tube, and centrifuged using an Eppendorf Centrifuge 5417R at 8000 rpm for 1 min.

c. Analytical Methods

PXRD data was acquired using a Bruker D8-Advance X-ray diffractometer in Bragg-Brentano configuration with Copper $K\alpha_1$ and $K\alpha_2$ radiation sources. A Nickel filter was used to filter out the CuKβ line. The detector was a LynxEye silicon strip and the generator was 40 kV and 40 mA. The slits used were 1 mm divergent, 8 mm anti-scatter and 2.5° soller. Samples were powder packed in a standard Bruker sample holder and were not rotated. Scans were plotted using HighscorePlus (Malvern-Panalytical).

HPLC analysis was performed on an Agilent 1290 Infinity HPLC equipped with DAD detector. The collected samples were analyzed using the following chiral method:

Daicel OD-3 Chiralcel Column, 4.6 x 250 mm; 3 µm
Solvent A = Water (10 mM NH_4OAc); Solvent B = Acetonitrile
Flow Rate = 0.650 mL/min
Column Temperature = ambient (25 °C)
Sample Loop Volume = 100 µL
Gradient: A:B 40:60 – initial (isocratic)
11 min stop time, no post time

The collected samples were also analyzed using the following achiral method:

Agilent EC-C18 Guard Column, 3.0 x 5 mm, 1.9 µm
Agilent Poroshell 120 EC-C18 Column, 2.1 x 50 mm; 2.7 µm
Solvent A = Water (0.1% TFA v/v); Solvent B = Acetonitrile
Flow Rate = 0.600 mL/min
Column Temperature = ambient (25 °C)
Sample Loop Volume = 100 µL
Gradient: A:B 90:10 – initial
A:B 0:100 – 8 min
9 min stop time, 2 min post time

2. System Hardware

a. System Configuration

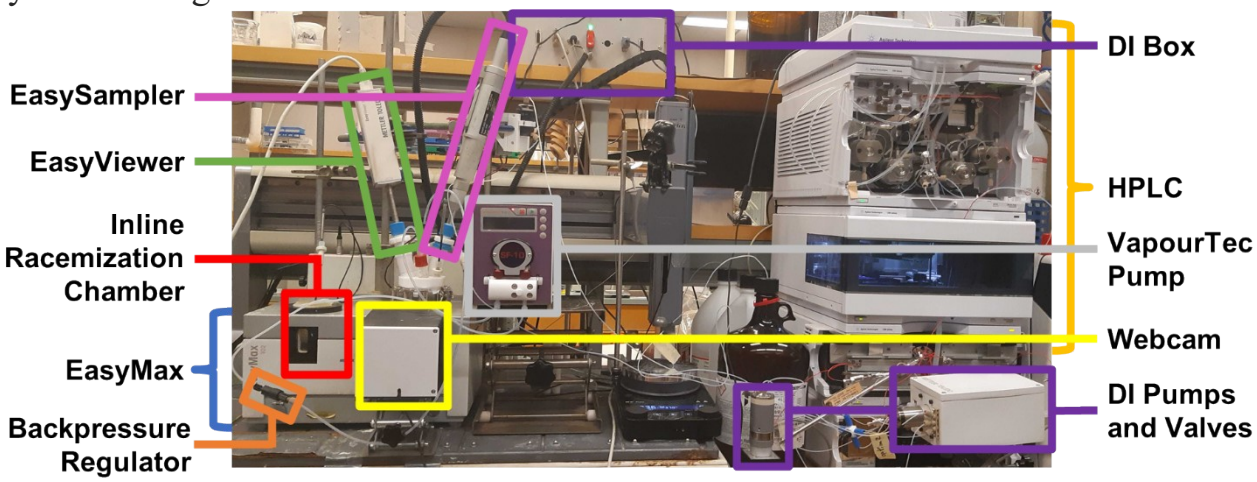

Figure SI 1. System configuration for inline racemization, showing the EasyMax containing the inline racemization chamber and reaction vessel (behind the webcam, which was used to allow the user to remotely monitor a reaction). Real-time solution concentrations were monitored by online HPLC using an EasySampler to take samples, and a custom-built control module (DI Box) to control sample acquisition and send samples via a series of pumps and valves to the HPLC for immediate analysis. Turbidity and particle images were tracked using an EasyViewer probe in the reaction vessel. Inline racemization was achieved by using the VapourTec pump to pull the solution phase through an inline filter, into the pump, through the inline racemization chamber and backpressure regulator, and then back into the reaction flask. In batch mode, the same setup was used but without the VapourTec pump, inline racemization chamber and backpressure regulator.

b. Inline Racemization Chamber

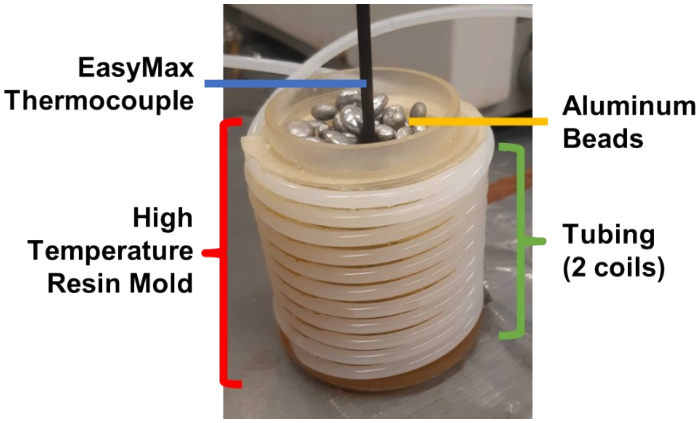

Figure SI 2. Inline racemization chamber consisting of two coils of 1/8" OD x 1/16" ID IDEX ETFE tubing wrapped around a 3D printed cylinder. Mold was printed using Formlabs high temperature resin. Grooves keep tubing in place such that the assembly can be inserted inside the reactor well of an EasyMax 102 Advanced Thermostat unit. Total tubing volume was 7.4 mL between pump #2 and the 20 PSI backpressure regulator located after the coil to allow elevated temperatures for racemization. The chamber contains two coils of tubing (one nestled underneath the other), each with a pitch of 10 turns over 5.0 cm. Inner coil diameter (Dc) is 5.06 cm (Dc/ID = 1.62), outer coil diameter is 5.7 cm (Dc/ID = 1.82).

3. Synthetic Procedures

a. Freebasing (*S*)-**1**•L-DBTA

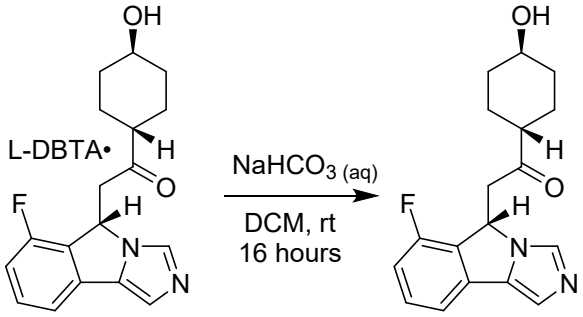

(S)-**1**•L-DBTA *(S)*-**1**

To a 500 mL round bottom flask equipped with a stir bar were added (*S*)-**1**•L-DBTA (28.7 g, 42.6 mmol), saturated aqueous sodium bicarbonate solution (220 mL) and dichloromethane (DCM, 160 mL). The mixture was stirred vigorously for 16 hours at room temperature, then the layers were separated and the organic layer washed with water (50 mL). The organic layer was then dried with $MgSO_4$, filtered and solvent removed *in vacuo* to afford (*S*)-**1** as an off-white crystalline solid (12.4 g, 39.4 mmol, 92.6% yield).

b. Racemizing and Recrystallizing (*S*)-**1** into *rac*-**1**

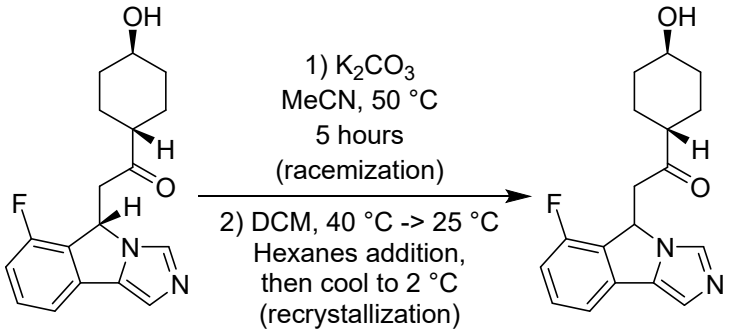

(S)-**1** *rac*-**1**

To a 250 mL round bottom flask was added (*S*)-**1** (8.00 g, 25.4 mmol), acetonitrile (75 mL) and K_2CO_3 (840 mg, 6.08 mmol). The mixture was stirred vigorously at 50 °C for 5 hours, then cooled to room temperature. The mixture was filtered and washed with DCM (30 mL) to dissolve all solids but the K_2CO_3, and solvent removed *in vacuo* to afford a yellow solid. This solid was then transferred to a 100 mL EasyMax flask using hot DCM (30 mL), and the mixture stirred at 40 °C. DCM (15 mL) was then added until all solids dissolved at 40 °C. The solution was then cooled rapidly to 25 °C, and hexanes antisolvent addition (70 mL) was performed *via* a dosing unit at a rate of 1 mL/min. The flask was then cooled to 2 °C at 0.5 K/min and stirred overnight. Filtering while rinsing with hexanes afforded purified *rac*-**1** as an off-white solid (7.99 g, 25.3 mmol, >99% yield).

c. Synthesizing (*S*)-**1**•L-DBTA from *rac*-**1**

Prepared according to the previously reported procedure by St-Jean *et al.* with matching spectroscopic and spectrometric data.[2] The procedure was replicated at three scales smaller than that originally reported (2.00 g, 5.00 g and 10.00 g of *rac*-**1**) to afford off-white solids (3.00 g, 70% yield, 90% e.e.; 8.68 g, 81% yield, 91% e.e.; and 18.21 g, 85% yield, 93% e.e.). See SI section 7f for scale reproducibility discussion.

4. Calibration and Standard Additions

a. Background

Standard additions were performed at the beginning of as many experiments as possible to minimize variation from experiment to experiment and to ensure accurate quantitation of analytes during each experiment. This method involves adding known quantities of reagent to produce an internal calibration curve during each experiment, allowing accurate quantitation and circumventing the impact of matrix effects (which would hamper the applicability of a standard external calibration curve being used for all experiments). To calibrate each analyte (when applicable), standard addition(s) were performed for *rac*-**1** at the beginning of each experiment and for L-DBTA at the end.

Analytes **3** and **4** (the major undesired decomposition products of **1** and L-DBTA, respectively) were assumed to have very similar instrumental response factors to **1** and L-DBTA due to minimal structural changes. As such, the standard additions of **1** and L-DBTA were used to quantitate these components' concentrations. Quantitation for each analyte was performed using the wavelength that provided the highest possible signal without maxing out the detector. When standard additions could not be performed, the calibration curve from the most recent experiment at the same wavelength was used to quantify the analytes.

b. Procedure

At the start of every experiment, at least two solvent blanks were acquired using online HPLC. *Rac*-**1** was then added in no less than two portions such that both portions completely dissolved, resulting in an experiment-specific calibration curve with at least two data points. The slope of this calibration curve could then be used to convert all raw peak area values from the online HPLC data into concentration data, allowing analyte concentration vs. time to be plotted. If L-DBTA was also to be quantified, then standard addition(s) were performed after the experiment was deemed complete. However, since L-DBTA would crystallize and/or decompose in the reaction solution in the presence of **1**, calibration curves could not be created. Instead, the increase in signal from the previous timepoint to after the L-DBTA addition was used to calibrate the detector response to L-DBTA. If multiple L-DBTA additions were performed, then the detector responses were averaged in order to determine the response factor and convert the peak areas to concentration data.

c. Sample Raw Data – Testing Inline Racemization (Achiral)

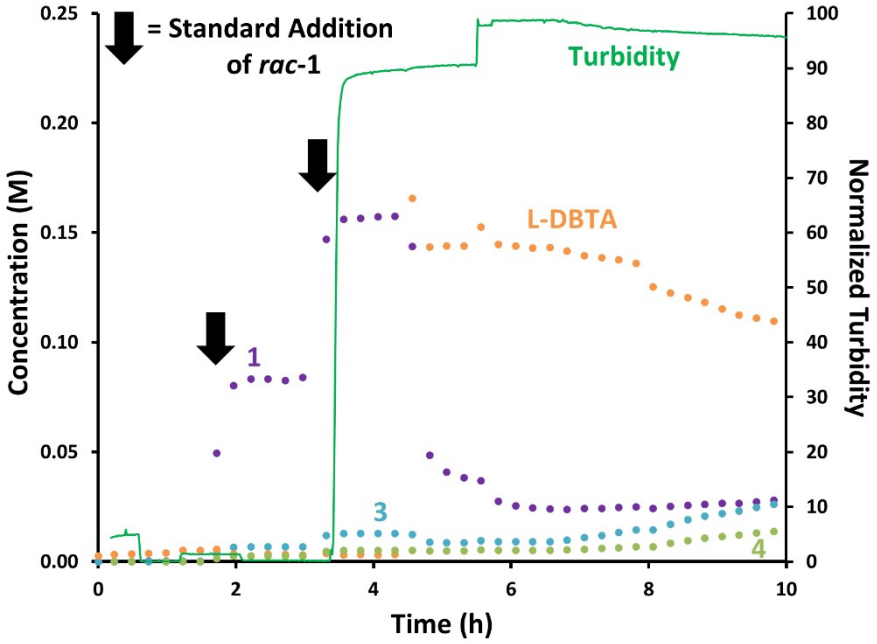

Figure SI 3. Sample standard addition raw data from end of experiment testing inline racemization (monitoring with achiral column). Standard additions are noted with black arrows: 1.50 g of *rac*-**1** were added at 2 h and 3 h after initial solvent blanks were acquired.

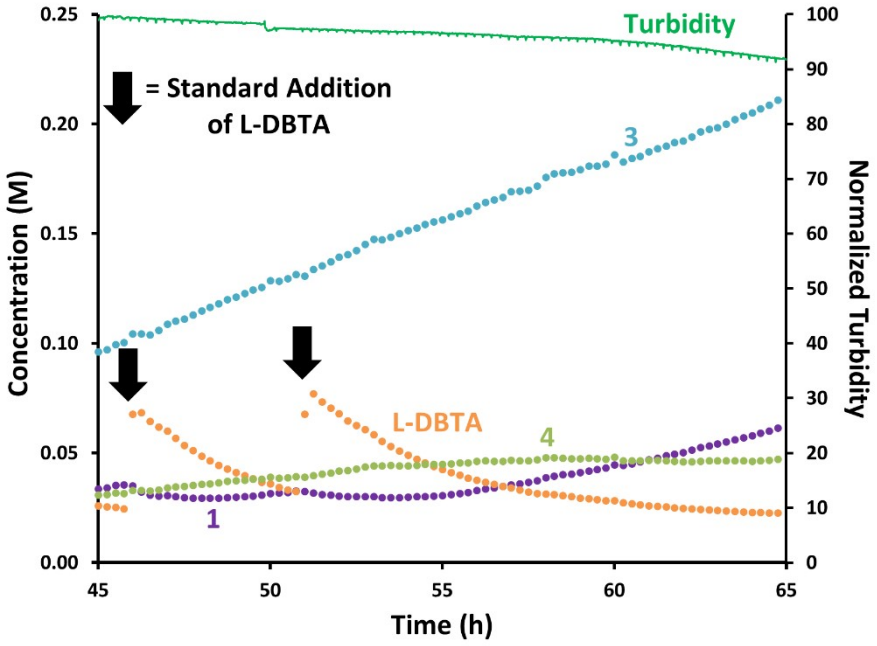

Figure SI 4. Sample standard addition raw data from end of experiment testing inline racemization (monitoring with achiral column). Standard additions are noted with black arrows: 1.00 g of L-DBTA were added at 46 h and 51 h, with the crystallization and decomposition of L-DBTA resulting in different behaviour from the *rac*-**1** standard additions at the beginning of the experiment.

d. Sample Calibration Curves – Testing Inline Racemization

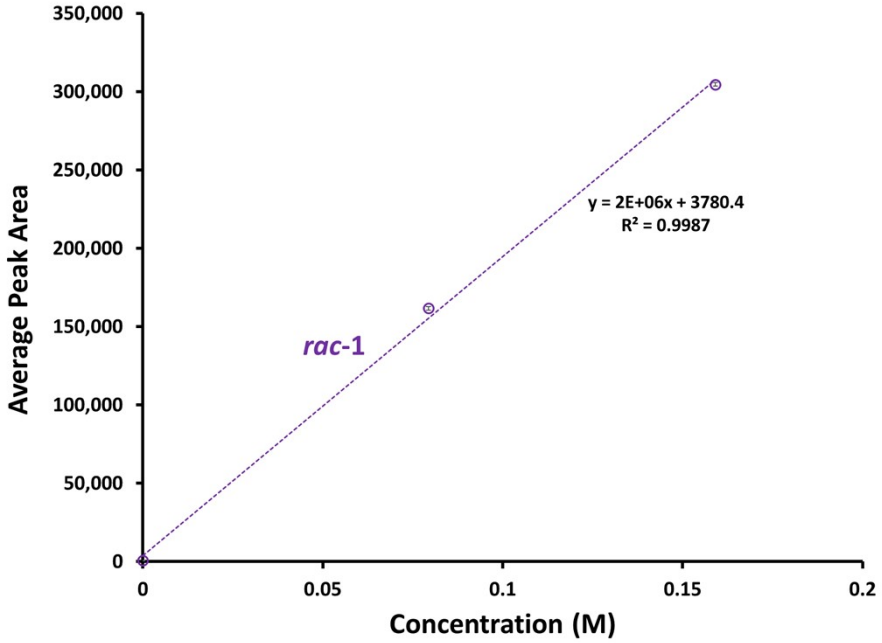

Figure SI 5. Calibration curve generated by averaging standard addition raw data signals for *rac*-**1** after concentration was observed to plateau.

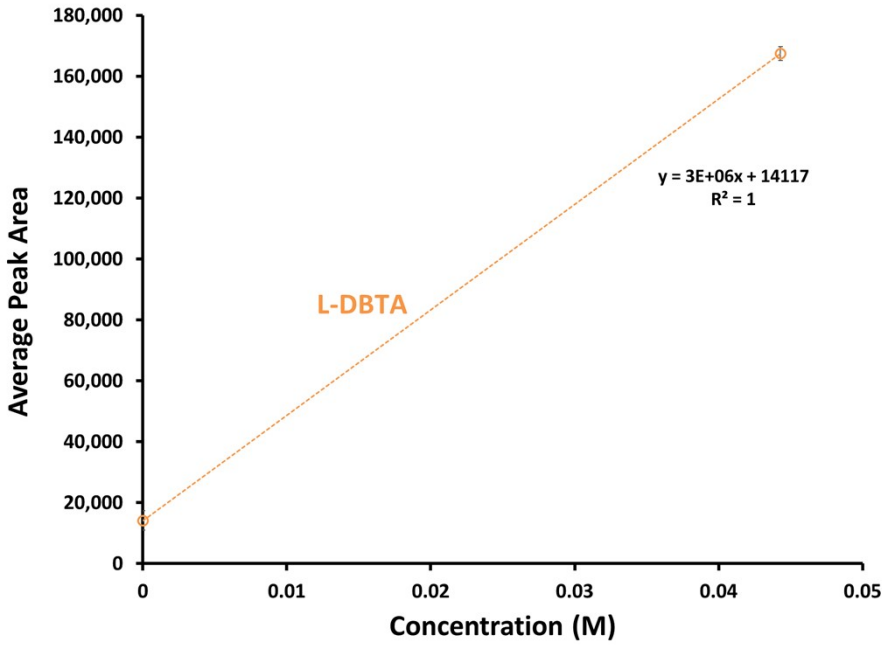

Figure SI 6. Calibration curve generated by averaging the increase in peak area observed after 1.00 g of L-DBTA was dosed into the solution as a standard addition.

5. Experimental Procedures

a. General Manual Sampling Procedure

Manual solid and solution phase sampling were performed using a micropipette and a centrifuge. Before taking a sample, the lower 3 mm of a 1 mL micropipette tip was removed to allow larger particles to be sampled than would otherwise be possible with an unmodified micropipette. To acquire a sample, ~500 µL of solution (no longer calibrated precisely due to the change in tip geometry) was transferred to a centrifuge vial *via* micropipette. This sample was immediately centrifuged at 8000 rpm for 1 minute. After centrifugation, a portion of the solids was transferred to an HPLC vial and dissolved in ~1 mL EtOH, while the solution phase was transferred to a separate HPLC vial and diluted to ~1 mL with EtOH. Both vials were then submitted for offline chiral HPLC analysis to determine each phase's e.e.

b. L-DBTA Undercharge CIDT Procedure – Figure 4 and Figure SI 10

To a 100 mL EasyMax flask equipped with a cross-shaped stir bar was added 30 mL EtOH. The flask was heated to 70 °C and *rac*-**1** (10.0 g, 31.8 mmol) was added. A solution of L-DBTA in EtOH at 70 °C (0.97 M, 30.0 mL, 0.92 equiv) was then added over three minutes, followed by a slurry of *rac*-**1**•L-DBTA solids (0.1 g) in EtOH (0.5 mL) to act as seed crystals. The solution was stirred at 200 rpm at 70 °C for 11 hours, and then cooled to 20 °C at 0.5 K/min. The solution was then held at 20 °C for 5.5 hours, after which the (*S*)-**1**•L-DBTA solids were isolated by suction filtration as an off-white powder (13.65 g, 64% yield, 96% e.e.).

c. Testing Inline Racemization (Achiral) – Figure 6 and Figures SI 3, 4, 5, 6 and 11

To a 100 mL EasyMax flask equipped with a cross-shaped stir bar was added 60 mL EtOH. The flask was heated to 35 °C, stirred at 200 rpm, and online sampling with HPLC was started. After 7 solvent blanks, *rac*-**1** (1.50 g, 4.77 mmol) was added as a first standard addition and 6 online HPLC samples acquired. Another standard addition of *rac*-**1** (1.50 g, 4.77 mmol) was performed, 5 more samples taken, and then L-DBTA (5.60 g, 14.9 mmol) was added. After 3 hours, a manual sample was acquired and inline racemization begun (*via* turning on the VapourTec pump at 1 mL/min). An additional manual sample was acquired after 11 hours, followed by a third after 7 more hours and a fourth after 9 hours. Following a sampling error occurring for ~9 hours, sampling was resumed and two standard additions of L-DBTA (1.00 g, 2.66 mmol) were performed. Sampling was then ended after 14 additional hours of sampling, and the off-white (*S*)-**1**•L-DBTA solids isolated by suction filtration (1.85 g, 29% yield, 83% e.e.).

d. Testing Inline Racemization (Chiral) – Figure 7 and Figure SI 12

To a 100 mL EasyMax flask equipped with a cross-shaped stir bar was added 60 mL EtOH. The flask was heated to 35 °C, stirred at 200 rpm, and online sampling with HPLC was started. After 4 solvent blanks, *rac*-**1** (1.50 g, 4.77 mmol) was added as a first standard addition and 4 online HPLC samples acquired. Another standard addition of *rac*-**1** (1.50 g, 4.77 mmol) was performed, 5 more samples taken, and then L-DBTA (5.60 g, 14.9 mmol) was added. The solution was then rapidly heated to 70 °C and then cooled to 20 °C in an unsuccessful attempt to selectively dissolve and/or crystallize just one enantiomer. Inline racemization was begun (*via* turning on the VapourTec pump), first at 0.6 mL/min and then adjusted to 1 mL/min after 5 hours. A manual sample was acquired 27 hours after adjusting the flow rate to 1 mL/min. The next day, sampling was ended and the solution filtered to afford off-white (*S*)-**1**•L-DBTA solids (3.64 g, 57% yield, 83% e.e.).

e. Genentech CIDT Procedure (Chiral) with Inline Racemization – Figures 2 and 9, and Figure SI 7 and 8

To a 100 mL EasyMax flask equipped with a cross-shaped stir bar was added 30 mL EtOH. The flask was heated to 70 °C and stirred at 500 rpm, and the solution sampled repeatedly via online HPLC before *rac*-**1** (2.50 g, 7.95 mmol) was added as a first standard addition. After 5 samples were acquired, another standard addition of *rac*-**1** (2.50 g, 7.95 mmol) was added. 5 more samples were acquired, then another portion of *rac*-**1** (5.00 g, 15.9 mmol) was added. A solution of L-DBTA in EtOH at 50 °C (1.08 M, 41.3 mL, 1.4 equiv) was then added over two minutes, and a manual sample was acquired. The solution was continued to stir at 500 rpm at 70 °C for 8 hours, with manual samples acquired 0.5, 1, 2, 4, and 8 hours after L-DBTA addition. The solution was then cooled to 20 °C at 0.5 K/min, held at 20 °C for 2 hours, and then inline racemization was begun (*via* turning on the VapourTec pump at 1 mL/min). After 6 hours, a final manual sample was acquired and (*S*)-**1**•L-DBTA solids were then isolated by suction filtration as an off-white powder (17.86 g, 83% yield, 90% e.e.).

f. Genentech CIDT Procedure (Achiral) with Inline Racemization – Figures 3 and 8, and Figure SI 9

To a 100 mL EasyMax flask equipped with a cross-shaped stir bar was added 30 mL EtOH. The flask was heated to 70 °C and stirred at 500 rpm, and the solution sampled twice via online HPLC before *rac*-**1** (2.49 g, 7.92 mmol) was added as a first standard addition. After 4 samples were acquired, another standard addition of *rac*-**1** (2.50 g, 7.95 mmol) was added. 5 more samples were acquired, then another portion of *rac*-**1** (5.00 g, 15.9 mmol) was added. A solution of L-DBTA in EtOH at 50 °C (1.08 M, 41.3 mL, 1.4 equiv) was then added over two minutes, and a manual sample was acquired. The solution was continued to stir at 500 rpm at 70 °C for 8 hours, with manual samples acquired 0.5, 1, 2, 4, and 8 hours after L-DBTA addition. The solution was then cooled to 20 °C at 0.5 K/min, held at 20 °C for 2 hours, and then inline racemization was begun (*via* turning on the VapourTec pump at 1 mL/min). After 10 hours, a final manual sample was acquired the VapourTex flow rate was increased to 3 mL/min. After 5 hours of little change, L-DBTA (0.980 g, 2.60 mmol) was added in a standard addition. After 2 more hours, a final L-DBTA standard addition (0.994 g, 2.64 mmol) was performed, the solution was stirred for 2 hours, and (*S*)-**1**•L-DBTA solids were finally isolated by suction filtration as an off-white powder (17.52 g, 82% yield, 91% e.e.).

6. Expanded Experimental Data

a. Genentech CIDT Procedure (Chiral) with Inline Racemization – Figures 2 and 9

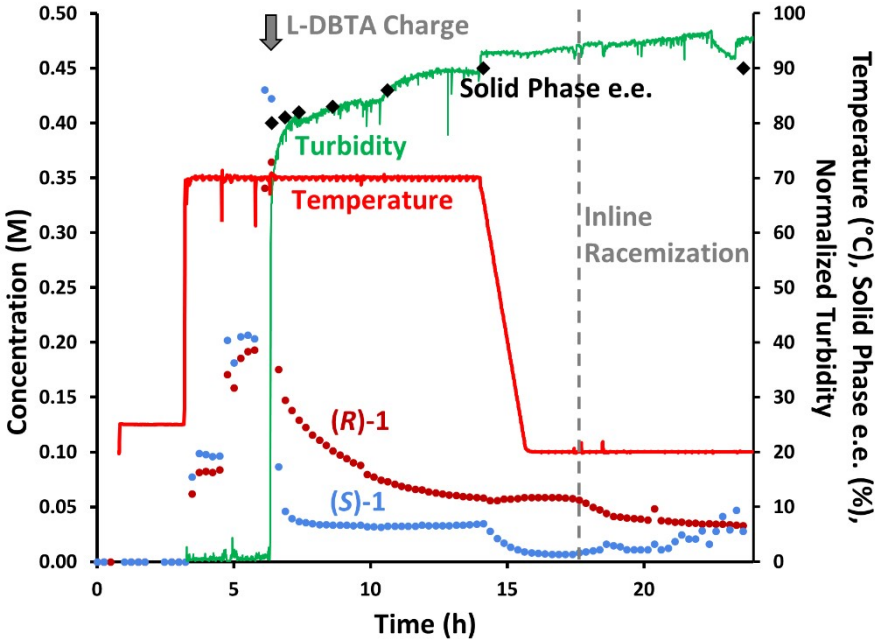

Figure SI 7. Full time course data for Figures 2 and 9, including initial solvent blanks, standard additions of *rac*-**1** before L-DBTA addition (time = 0 h in Figures 2 and 9) and normalized turbidity trend. *(R)*-**1** and (*S*)-**1** were analyzed at 254 nm to avoid detector signal saturation.

b. Comparison of Total (*R*)-**1** and (*S*)-**1** Trends from Figures 8 (Achiral) and 9 (Chiral)

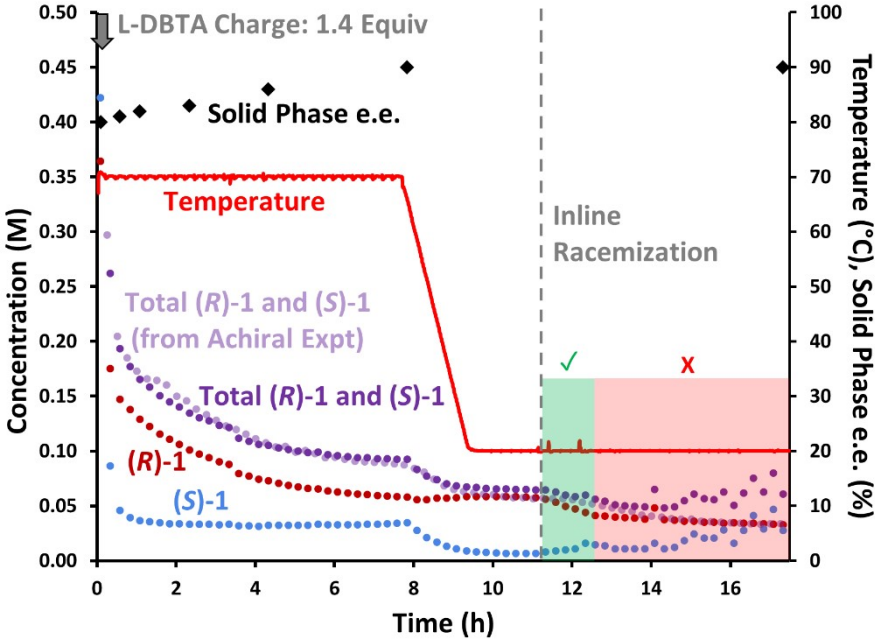

Figure SI 8. Comparison of total *(R)*-**1** and (*S*)-**1** trends from chiral monitoring (dark purple, sum of *(R)*-**1** and (*S*)-**1** trends from Figure 9) and achiral monitoring (light purple, from Figure 8) showing excellent agreement between the two sets of data.

c. Genentech CIDT Procedure (Achiral) with Inline Racemization – Figures 3 and 8

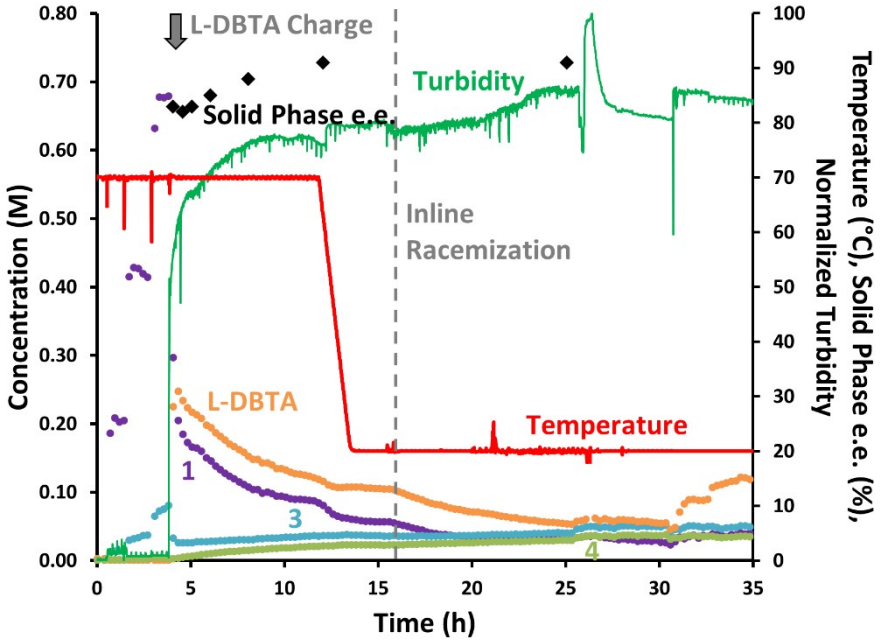

Figure SI 9. Full time course data for Figures 3 and 8, including initial solvent blanks, standard additions of *rac*-**1** before L-DBTA addition (time = 0 h in Figures 3 and 8), L-DBTA standard additions at the end of the experiment, and normalized turbidity trend. *Rac*-**1** and **3** were analyzed at 274 nm to improve low-concentration quantitation, and L-DBTA and **4** were analyzed at 254 nm to avoid detector signal saturation.

d. L-DBTA Undercharge CIDT – Figure 4

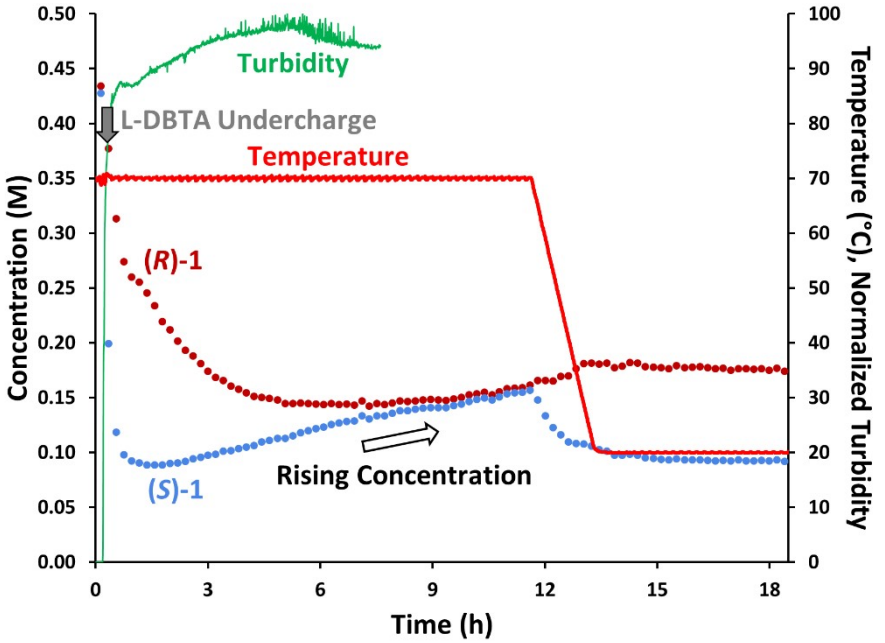

Figure SI 10. Figure 4 with added normalized turbidity trend (data acquisition ended after 8 hours). *(R)*-**1** and (*S*)-**1** were analyzed at 274 nm.

e. Testing Inline Racemization (Achiral) – Figure 6

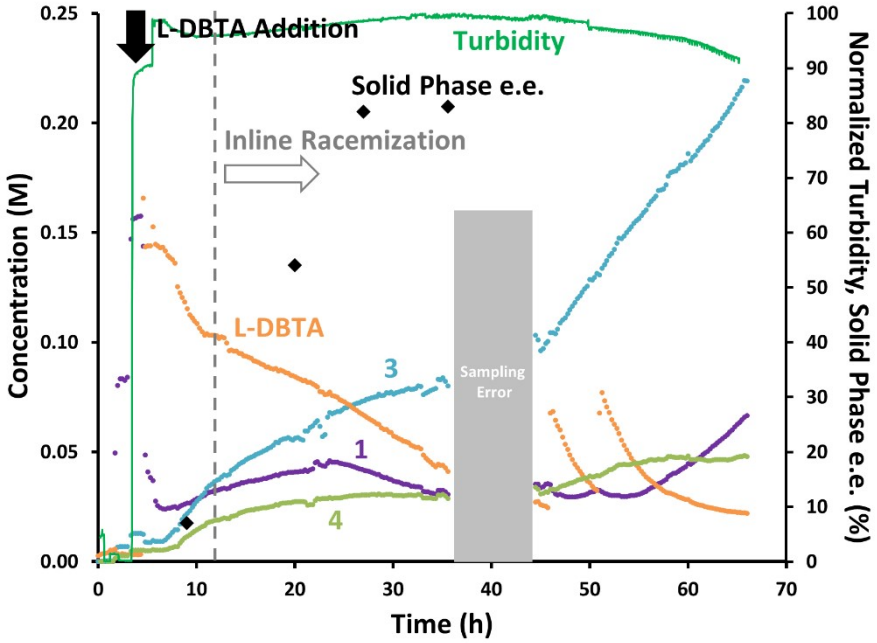

Figure SI 11. Full time course data for Figures 6, including initial solvent blanks, standard additions of *rac*-**1** before L-DBTA addition (time = 0 h in Figure 6), L-DBTA standard additions at the end of the experiment, and normalized turbidity trend. *Rac*-**1**, **3**, L-DBTA and **4** were analyzed at 220 nm to improve additional impurity detection.

f. Testing Inline Racemization (Chiral) – Figure 7

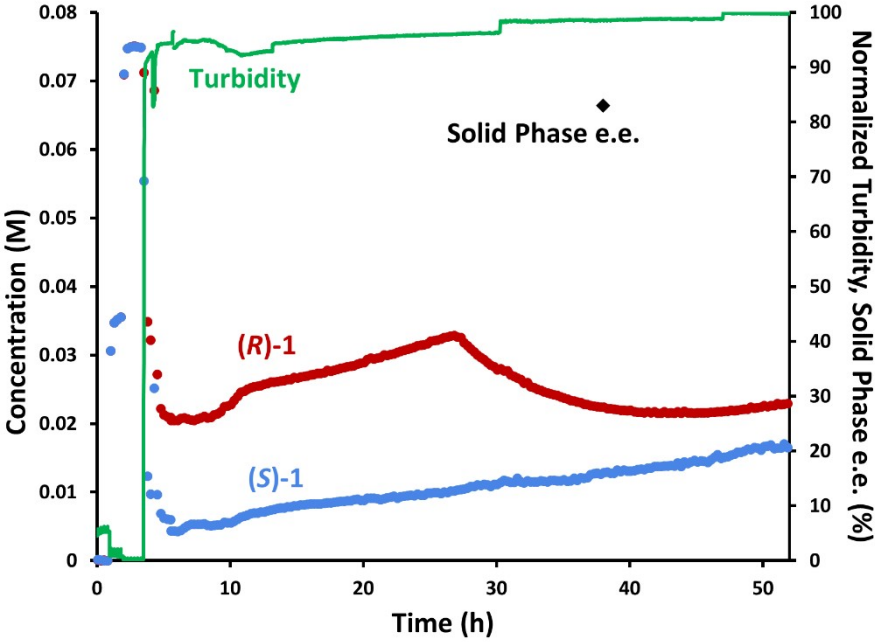

Figure SI 12. Full time course data for Figure 7, including initial solvent blanks, standard additions of *rac*-**1** before L-DBTA addition (time = 0 h in Figures 2 and 9) and normalized turbidity trend. *(R)*-**1** and (*S*)-**1** were analyzed at 274 nm.

7. Additional Experiments

a. Solubility Curves

Solubility curves for *rac*-**1** in EtOH and a mixture of (*R*)-**1** and (*S*)-**1** as their L-DBTA salts were obtained before beginning CIDT experimentation. In all cases, solids were added to EtOH at a low temperature such that the solution was saturated with both enantiomers. Online chiral HPLC was begun, and temperature was increased while monitoring each enantiomer's concentration in order to obtain their individual solubilities. The solvent was then evaporated and the solids were isolated and submitted for PXRD analysis (see SI section 10c and 10d).

Prior to the solubility curve for (*R*)-**1**•L-DBTA and (*S*)-**1**•L-DBTA in EtOH, *rac*-**1** was mixed with L-DBTA (1.00 equiv) in EtOH, stirred at room temperature, and the solvent removed under a stream of air to produce solids containing equal amounts of (*R*)-**1**•L-DBTA and (*S*)-**1**•L-DBTA.

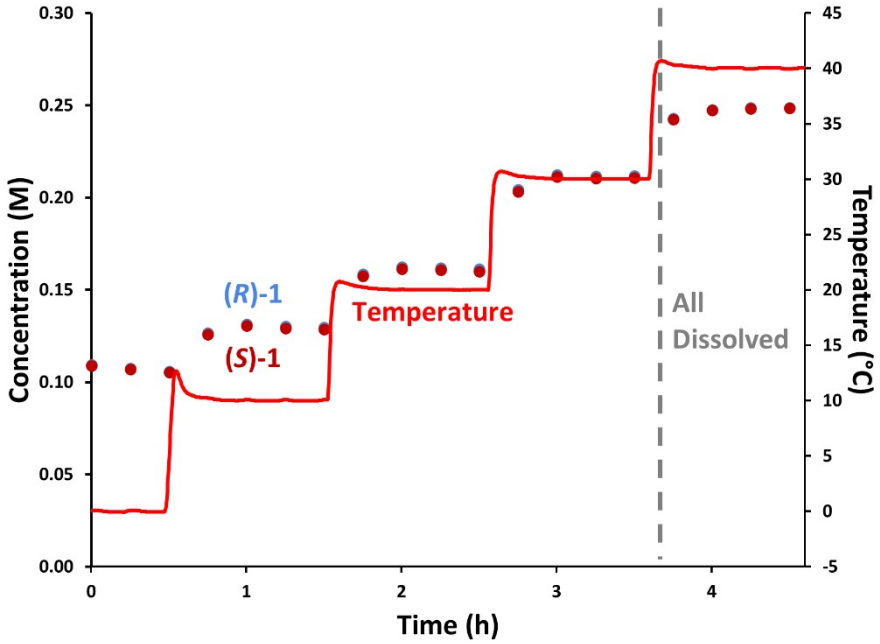

Figure SI 13. Full time course data for solubility of enantiomers of *rac*-**1** (9.44 g, 30.0 mmol) in EtOH (60 mL) at 0 °C, 10 °C, 20 °C and 30 °C. All solids dissolved at 40 °C, so the average peak area at this temperature for (*R*)-**1** and (*S*)-**1** was used as a single point calibration for the other temperatures (assuming 0.25 M per enantiomer at 40 °C). (*R*)-**1** data points overlap with (*S*)-**1** as expected from a racemic solution, and so are mostly obscured by the (*S*)-**1** trend. (*R*)-**1** and (*S*)-**1** were analyzed at 285 nm.

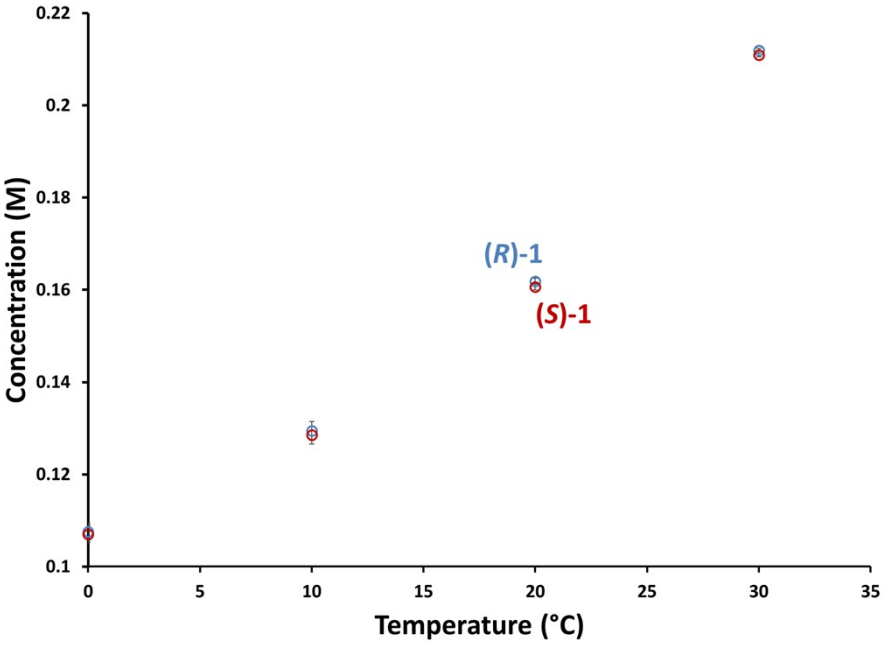

Figure SI 14. Solubility curve for (*R*)-**1** and (*S*)-**1** in EtOH from 0 °C to 30 °C, obtained from data in Figure SI 13.

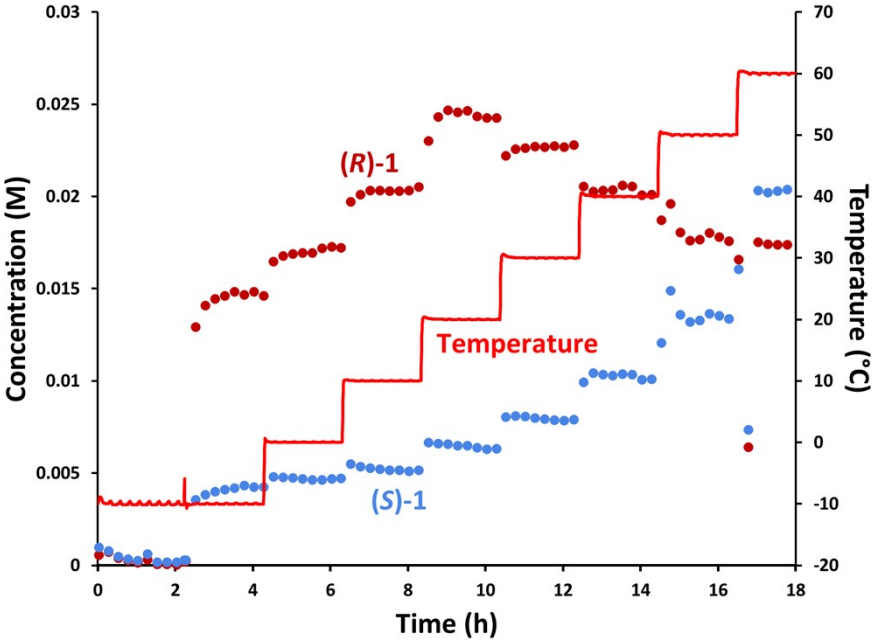

Figure SI 15. Full time course data for solubility of (*R*)-**1**•L-DBTA and (*S*)-**1**•L-DBTA salts in EtOH. A mix of (*R*)-**1**•L-DBTA and (*S*)-**1**•L-DBTA solids (2.90 g, 4.31 mmol) was added to EtOH (60 mL) after sampling at -10 °C for 2 hours to establish a solvent baseline. The solution was then heated in increments of 10 °C every 2 hours until 60 °C was reached. Solids persisted throughout, but the decreasing peak area of (*R*)-**1** above 20 °C suggests that enantiomer had fully dissolved (see SI section 7b for full discussion). As such, data from all temperatures was used for (*S*)-**1**•L-DBTA solubility but only data from 20 °C and below was used for (*R*)-**1**•L-DBTA solubility. (*R*)-**1** and (*S*)-**1** were analyzed at 274 nm.

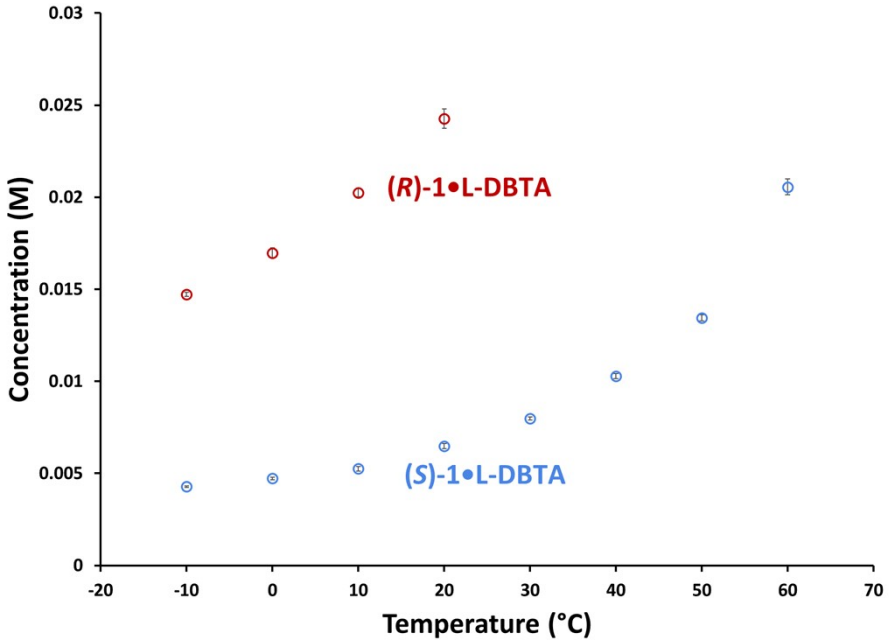

Figure SI 16. Solubility curves for (*R*)-**1**•L-DBTA and (*S*)-**1**•L-DBTA salts in EtOH from -10 °C to 60 °C, illustrating higher solubility of (*R*)-**1**•L-DBTA.

b. Signal Change with Temperature

In Figure SI 15 the concentration of (*R*)-**1** appears to decrease at temperatures beyond 20 °C. We propose this is due to a combination of all of the (*R*)-**1**•L-DBTA salt having dissolved (and thus the concentration not increasing at temperatures beyond 20 °C), and an observed decrease in signal at higher temperatures. If (*R*)-**1**•L-DBTA had fully dissolved, one would expect the concentration of (*R*)-**1** in solution to be unchanging (as it is saturated). However, the detector signal seems to be inversely proportional to temperature. This can be seen in Figures 2, 3, 8 and 9: when the solution is cooled from 70 °C to 20 °C, the concentration of (*R*)-**1** appears to increase slightly. However, manual sampling in Figures 8 and 9 confirms that no change in solid phase e.e. was observed before and after this temperature change, suggesting that (*R*)-**1** is not dissolving from the solid phase or otherwise increasing in concentration but is instead exhibiting this same signal change with temperature seen in Figure SI 15. This behaviour is also seen in SI section 7d as racemization is investigated at different temperatures.

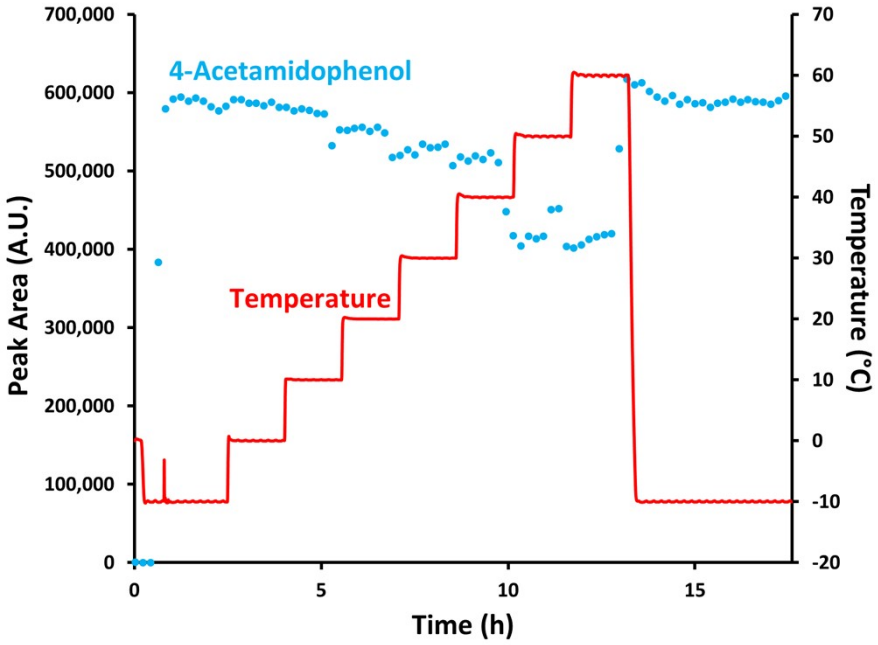

Figure SI 17. Changes in peak area of a homogeneous 0.25 M solution of 4-acetamidophenol in EtOH, sampled with a filter-modified EasySampler[1] from -10 °C to 60 °C. 4-Acetamidophenol was analyzed at 230 nm using the same achiral conditions as previous experiments.

We propose this change in signal with temperature is a result of the filter being used to obtain our online HPLC solution-phase samples. This filter works by creating alternating low and high pressure to pull solvent into its internal cavity (filling a 20 µL sample pocket) and then expelling the remaining solution as the sample is acquired.[1] Additionally, 20 µL of EtOH is dropped off within the filter's cavity during every sampling event. As such, changes in temperature may affect the degree to which the filter fills with and/or expels the reaction solvent, changing the effective dilution inside the filter and therefore the resultant peak area despite constant concentration. This was demonstrated in Figure SI 17, where a homogeneous 0.25 M solution of 4-acetamidophenol (2.27 g, 15.0 mmol) in EtOH (60 mL) was prepared at -10 °C, heated to 60 °C and cooled back to -10 °C. The peak area can be seen to decrease by as much as 33% (from 600,000 A.U. to 400,000 A. U.) when the solution is incrementally heated from -10 °C to 60 °C, and reproducibly returns to its original value (600,000 A.U.) upon cooling back to -10 °C. This suggests that this phenomenon is due to a systematic change in sampling across these temperatures.

As a result of these observations, standard additions for *rac*-**1** were performed at 70 °C for all CIDT experiments to ensure accurate quantitation during the CIDT portion of each experiment (before cooling). Given that higher peak areas were consistently observed at lower temperatures, this suggests that the calculated concentration data for rac-1 and 3 at 20 °C may be slightly higher than their actual values. Similarly, since L-DBTA standard additions were performed at 20 °C, this suggests that the solution concentrations of L-DBTA and 4 might be slightly underestimated during the 70 °C regime of each experiment. As this concentration data was only used to provide reaction trends and was not directly used for any kinetic calculations, the general trends of each component are unaffected by this signal change and thus correcting the data across the temperature range was deemed unnecessary.

c. Decomposition of L-DBTA and **1**

Given that F. St-Jean *et al.* previously observed decomposition of L-DBTA into its monoesterified product **4** (and additional debonzoylated side-products) within hours of adding L-DBTA into EtOH at 85 °C, we investigated the rate of reaction of L-DBTA in 70 °C EtOH at a similar concentration to that used in the CIDT (Figure SI 18). In the absence of **1**, very little decomposition was observed after heating for almost 24 hours at 70 °C. This suggests that L-DBTA alone in EtOH is rather stable, even at elevated temperatures.

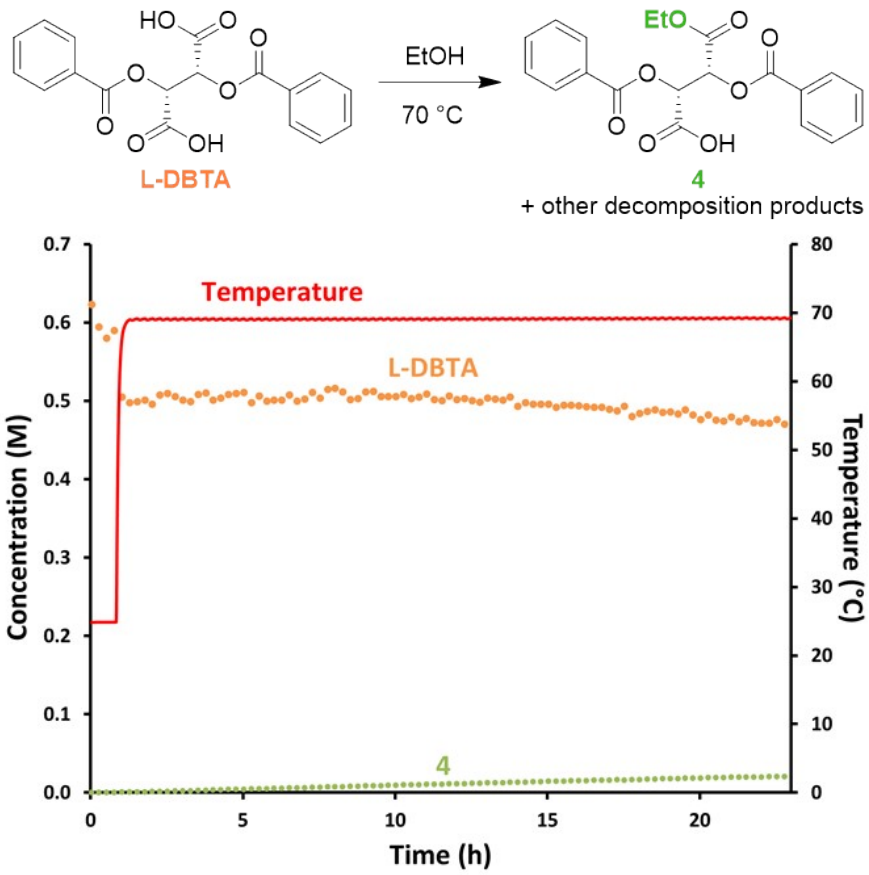

Figure SI 18. Decomposition of 0.61 M L-DBTA in EtOH into **4** at 70 °C in the absence of **1**.

However, analysis of the concentrated filtrate from a CIDT experiment (Figure SI 19) showed significant amounts of monoesterified product **4** (approaching the same concentration as L-DBTA) and many additional decomposition products of L-DBTA and **1**. With the use of positive and negative mode mass spectrometry in addition to achiral HPLC, all possible esterification products resulting from the carboxylic acid of L-DBTA reacting with EtOH were observed, as well transesterification of the benzoyl to ethyl benzoate (and therefore debenzoylation of the tartaric acid's hydroxyl group). In addition, the non-UV active species resulting from total debenzoylation of L-DBTA were observed as minor peaks in the mass spectrometer. The significant decomposition of L-DBTA in the presence of **1**, despite little decomposition in just EtOH, suggests that **1** may be playing a role as a nucleophilic catalyst for its decomposition.

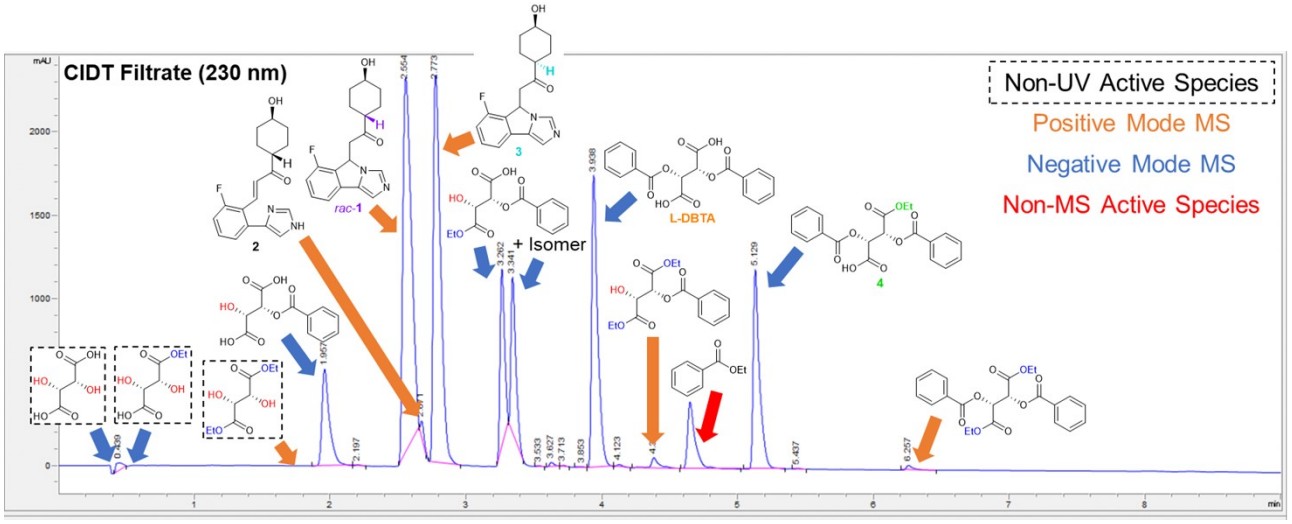

Figure SI 19. Assignment of compounds present (both UV active and inactive) in the filtrate of a CIDT reaction after concentration *in vacuo* and analysis *via* HPLC-MS using achiral conditions at 230 nm.

To confirm the identity of its suspected peak at 4.7 min (with no MS signal), ethyl benzoate was added to the mixture and found to elute at 4.7 min, confirming this peak's identity. While having no difference in mass, **3** was separated from **1** and confirmed by NMR to be the cis isomer at the cyclohexyl ring (see SI section 11). **2** was proposed to be the small peak eluting with **1** (at 2.7 min) due to its increased absorbance at higher wavelengths. This can be seen in Figure SI 20, where the only compound absorbing significantly at 310 nm is the peak at 2.7 min, as would be expected of the conjugated intermediate **2**.

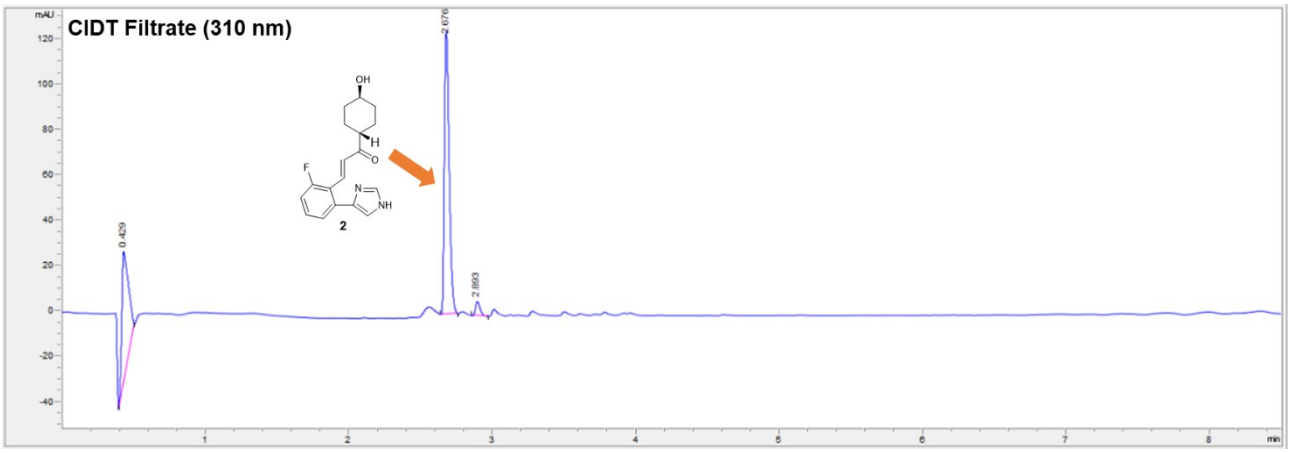

Figure SI 20. Assignment of **2** in the CIDT filtrate based on its absorbance at higher wavelengths. The chromatogram at 310 nm illustrates that it is the only species absorbing significantly at this wavelength.

d. Racemization of (*S*)-**1**

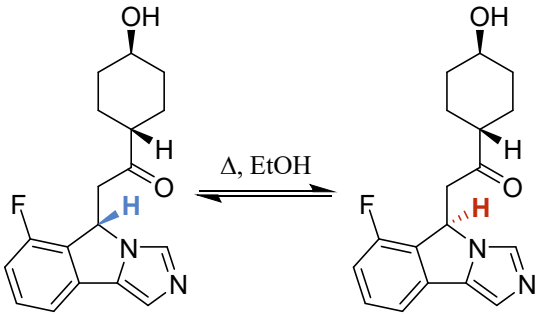

(*S*)-**1** (*R*)-**1**

To investigate the racemization of **1** with and without L-DBTA, solutions of one enantiomer of **1** in EtOH were heated while sampling with online chiral HPLC. Since L-DBTA gave us ready access to enantiopure (*S*)-**1** (following the procedure outlined in SI section 3a to obtain (*S*)-**1** from (*S*)-**1**•L-DBTA), we tested the racemization of (*S*)-**1** into *rac*-**1** under the assumption that racemization of (*R*)-**1** into *rac*-**1** would follow the same behaviour. This would later inform the design of our inline racemization conditions.

With no L-DBTA present, (*S*)-**1** (1.33 g, 4.23 mmol) was added to EtOH (20 mL) at 25 °C, rapidly heated to 40 °C to ensure all (*S*)-**1** dissolved, and then cooled to 0 °C (Figure SI 21). It was necessary to ensure that all (*S*)-**1** dissolved in order to observe its decrease in peak area with racemization, as a saturated solution with a solid phase may obscure any trends from racemization. Heating the homogeneous solution in increments of 10 °C to 70 °C showed the expected changes in signal with temperature (as discussed in SI section 7b). However, despite no L-DBTA present to act as an acid catalyst, some racemization was observed to begin at roughly 50 °C (best visualized in Figure SI 22 with only (*R*)-**1**). Additionally, higher temperatures were found to racemize (*S*)-**1** faster, suggesting that inline racemization may best be performed at temperatures even higher than 70 °C (see SI section 9).

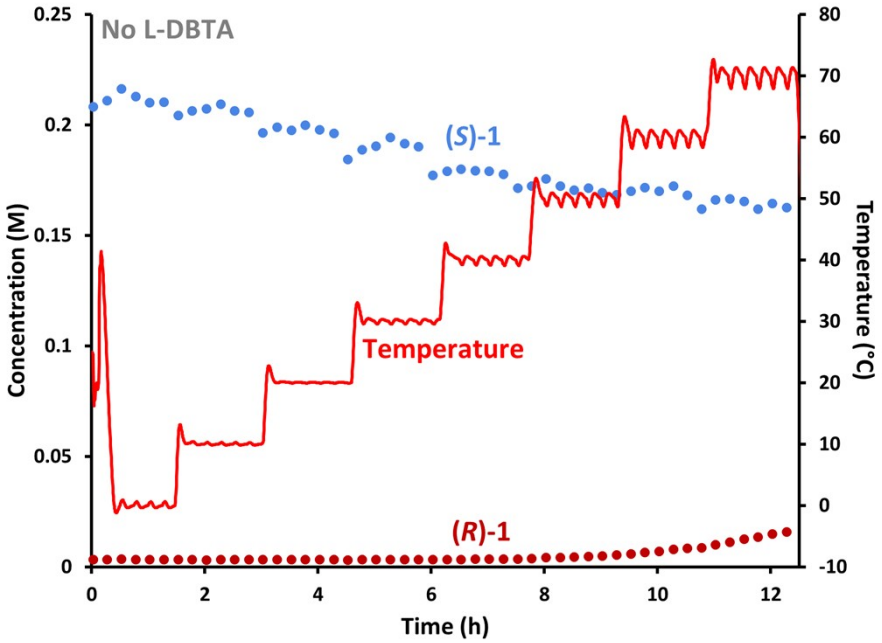

Figure SI 21. Monitoring 0.21 M (*S*)-**1** in EtOH with online chiral HPLC as it was heated, illustrating change in signal with temperature and racemization of (*S*)-**1** into (*R*)-**1** beginning at ~50 °C with no L-DBTA present.

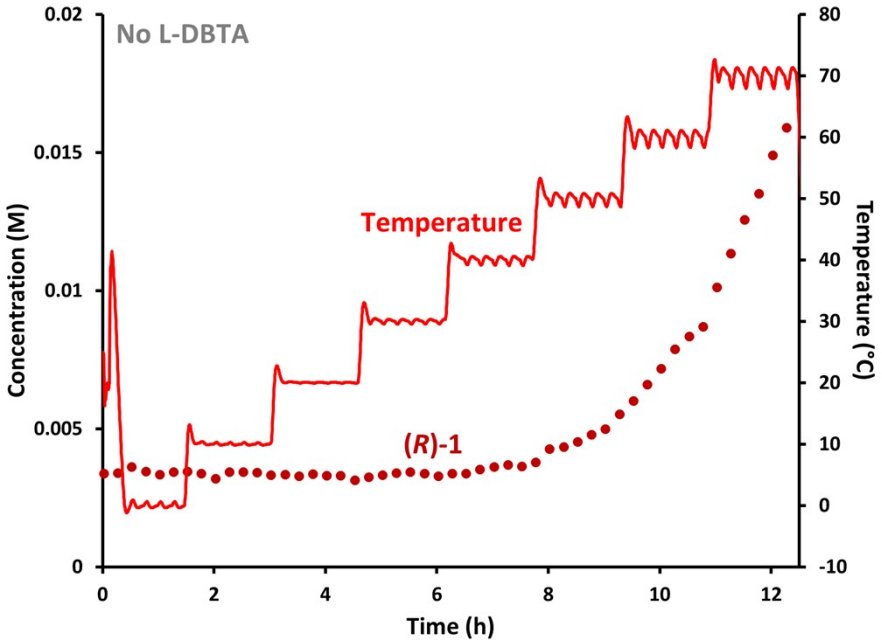

Figure SI 22. Zoomed in plot of (*R*)-**1** concentration from Figure SI 20, better emphasizing onset of racemization and increased rate at higher temperatures.

To then test racemization in the presence of L-DBTA, (*S*)-**1** (44 mg, 0.14 mmol) was added to EtOH (20 mL) at 20 °C, followed by L-DBTA (60 mg, 0.17 mmol, 1.2 equiv). Much like when no L-DBTA was present, racemization seems to start at around 50 °C, increasing rapidly with temperature (Figures SI 23 and 24). Given that this solution was far more dilute (due to the lower solubility of the L-DBTA salts) but still showed rapid racemization at higher temperatures, this confirmed that L-DBTA acts as an acid catalyst and increases the rate or racemization when it is present and suggested that higher equivalences be investigated for inline racemization (see SI section 9).

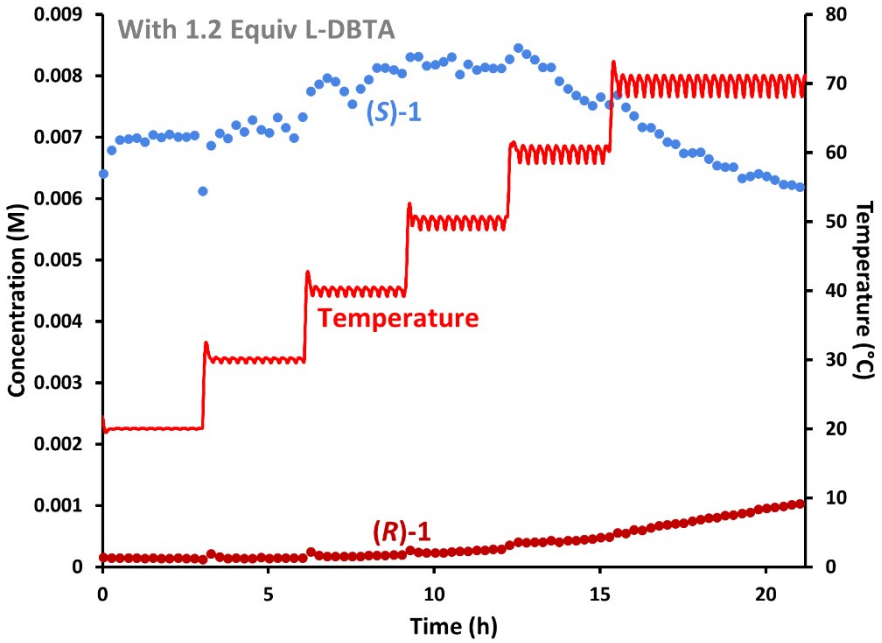

Figure SI 23. Monitoring 0.0070 M (*S*)-**1** in EtOH with online chiral HPLC as it was heated in the presence of 1.2 equiv L-DBTA, illustrating racemization of (*S*)-**1** into (*R*)-**1** beginning at ~50 °C.

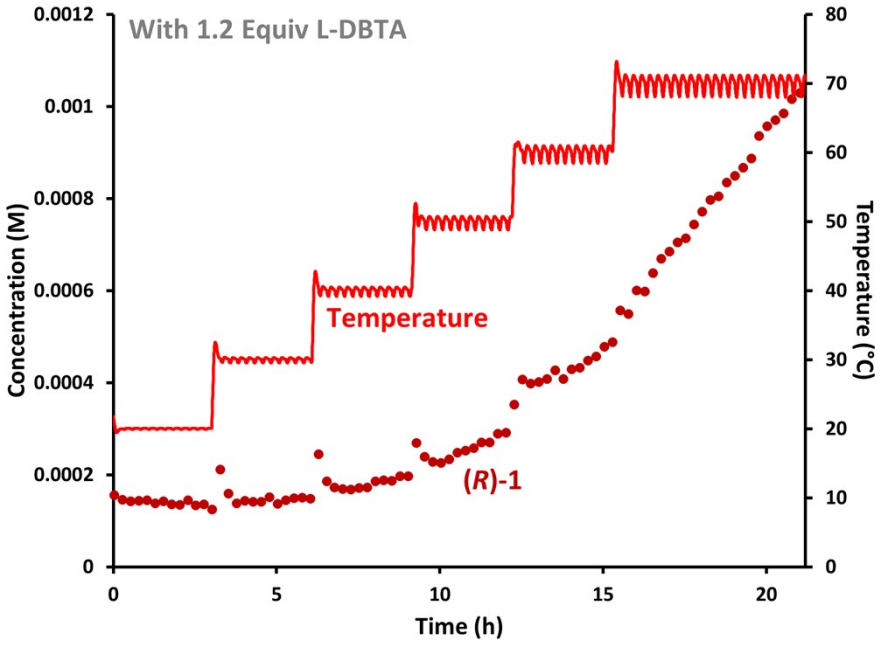

Figure SI 24. Zoomed in plot of (*R*)-**1** concentration from Figure SI 23, better emphasizing onset of racemization and increased rate at higher temperatures in the presence of 1.2 equiv of L-DBTA.

e. Solid Phase Impurity Incorporation Discussion: Rinsing CIDT Solids

In Figures 6 and 7, the solution phase of a slurry mixture of (*R*)-**1**•L-DBTA and (*S*)-**1**•L-DBTA in EtOH was passed through the inline racemization chamber. The solid phase manually sampled in these experiments exhibited a slow increase in e.e. from near 0% initially (*i.e.*, racemic) to a plateau of 82% e.e, as the solution phase (*R*)-**1** concentration trend experienced a dramatic change in slope. In the main text, this was proposed to be due to (*R*)-**1**•L-DBTA and (*S*)-**1**•L-DBTA forming separate solid phases with different solubilities (as seen in SI section 7a). As solution phase racemization of (*R*)-**1** into (*S*)-**1** occurred, the (*R*)-**1**•L-DBTA solids slowly dissolved and were converted into (*S*)-**1**•L-DBTA and crystallized out of solution. This is also supported by the PXRD data in SI section 10: the racemic solids used in these racemization experiments (Figure SI 38) shared many diffraction peaks with the PXRD pattern of enantiopure (*S*)-**1**•L-DBTA, but also contained some additional peaks that were not from (*S*)-**1**•L-DBTA (highlighted in yellow in Figure SI 39). This suggests that these racemic solids made from *rac*-**1** and L-DBTA contain two different solid phases: (*S*)-**1**•L-DBTA and presumably (*R*)-**1**•L-DBTA.

However, if (*R*)-**1** and (*S*)-**1** formed entirely different phases with L-DBTA, then solids would be expected to reach enantiopurity (*i.e.*, 100% e.e.) with extended racemization and to not plateau at only 82% e.e. Similarly, during the CIDTs shown in Figures 8 and 9 the solid phases manually sampled reached plateaus of ~90% e.e. and did not produce entirely enantiopure crystals. This suggests that some of the undesired (*R*)-**1**•L-DBTA may have been incorporated into the (*S*)-**1**•L-DBTA crystals and was not forming an entirely separate phase. Multiple mechanisms of impurity incorporation during crystallization exist including:

i) Supersaturation and phase separation (*i.e.*, what was proposed for (*R*)-**1**•L-DBTA and (*S*)-**1**•L-DBTA based on the data in Figures 6 and 7)

ii) Incomplete removal of a mother liquor and subsequent deposition of nonvolatile impurities during drying (*i.e.*, surface impurities)
iii) Kinetic incorporation of impurities in a growing crystal (*e.g.*, trapped in inclusions in the crystal)
iv) Thermodynamic incorporation of impurities into the crystal lattice itself (*e.g.*, as a solid solution).[3]

To distinguish if the (*R*)-**1**•L-DBTA impurities were simply on the surface of the (*S*)-**1**•L-DBTA crystals (ii) or being incorporated into them (iii or iv), rinsing experiments as outlined by Nicoud and Myerson[4] were performed on the solid phases manually sampled during the CIDT experiments depicted in Figures 8 and 9.

After following the manual sampling procedure outlined in SI section 5a (involving acquiring, centrifuging and analyzing a portion of the solids *via* chiral HPLC), the filtrate from each centrifuge tube was also analyzed *via* chiral HPLC to determine the e.e. of the solution. The manual analysis data for the solids and solution from Figure 8 are plotted in Figure SI 25 and 26, respectively, and the data for the solids and solution from Figure 9 are plotted in Figure SI 27 and 28, respectively. After separating and analyzing the solids and solution, ~300 μL of EtOH was added to the remaining solids and they were agitated for ~1 minute with a spatula. The mixture was again centrifuged, and the solution and a portion of the solids were analyzed by HPLC (denoted the first rinse). This rinsing procedure was repeated up to the third rinse.

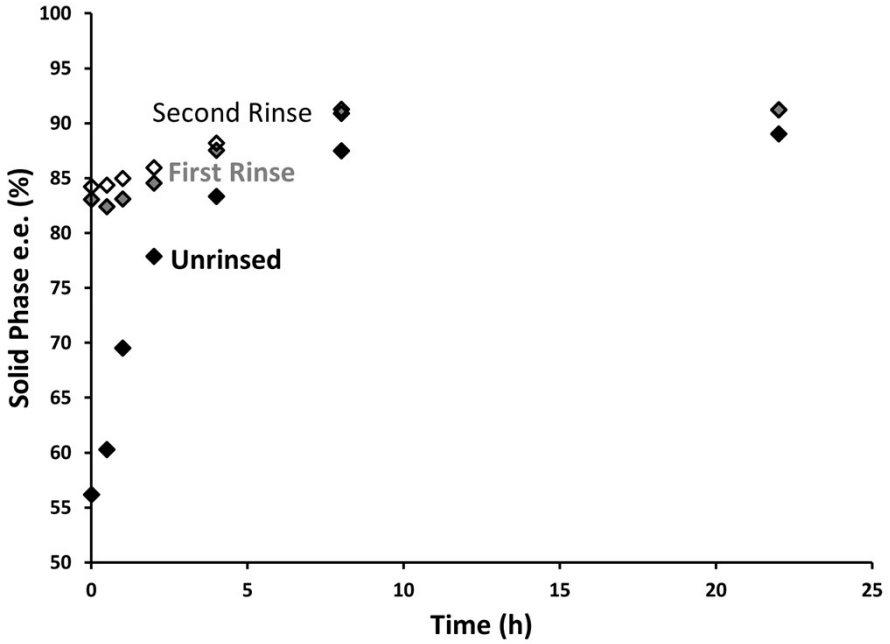

Figure SI 25. Effect of rinsing on e.e. of solid phase samples from achiral monitoring of CIDT experiment with inline racemization (Figure 8 and Figure SI 9), illustrating converging e.e. as more rinses were performed.

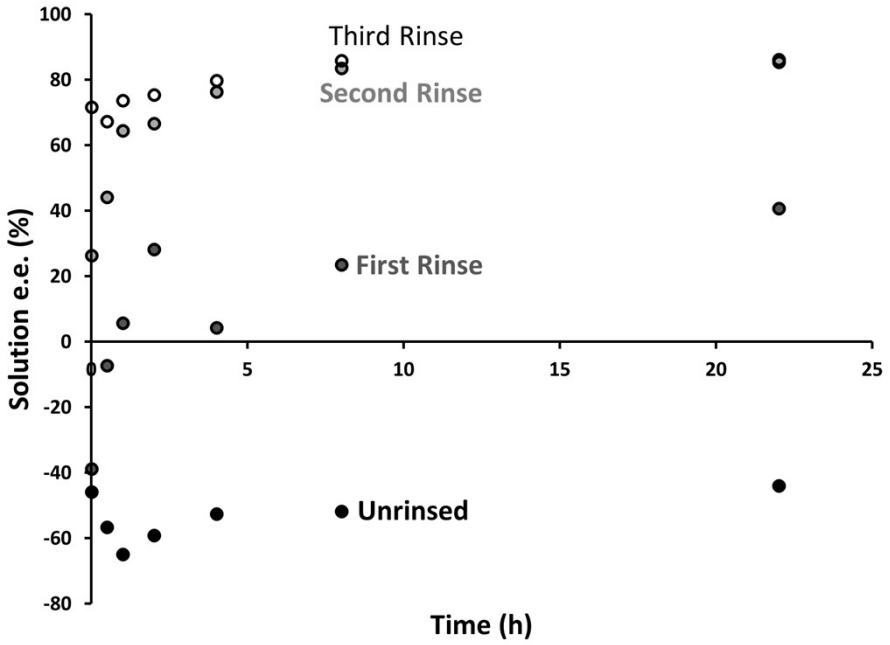

Figure SI 26. Effect of rinsing on e.e. of solution for samples from achiral monitoring of CIDT experiment with inline racemization (Figure 8 and Figure SI 9), illustrating converging e.e. as more rinses were performed.

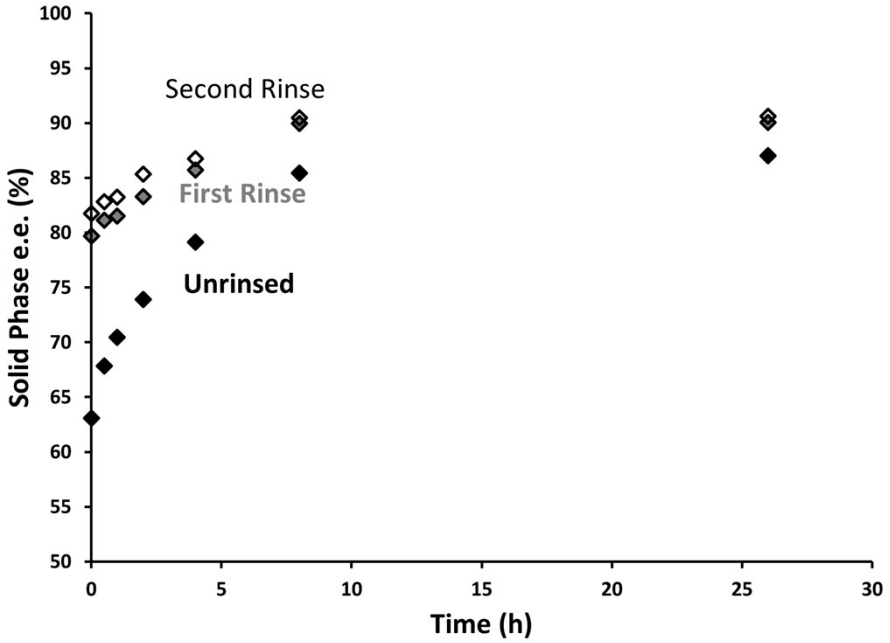

Figure SI 27. Effect of rinsing on e.e. of solid phase samples from chiral monitoring of CIDT experiment with inline racemization (Figure 9 and Figures SI 7 and 8), illustrating converging e.e. as more rinses were performed.

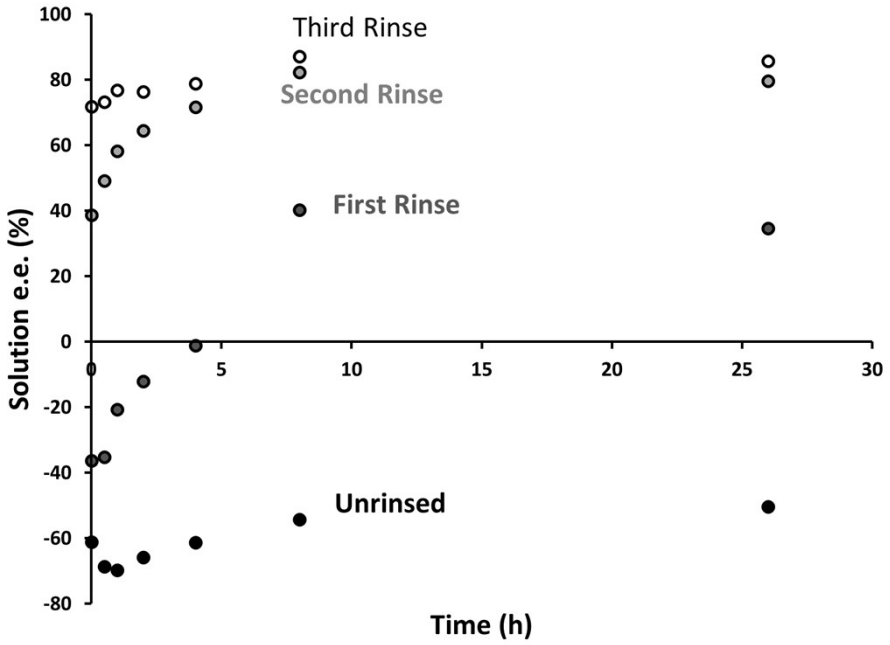

Figure SI 28. Effect of rinsing on e.e. of solution for samples from chiral monitoring of CIDT experiment with inline racemization (Figure 9 and Figures SI 7 and 8), illustrating converging e.e. as more rinses were performed.

For both solid phase analyses (Figures SI 24 and 26), the initial solids sampled at the beginning of the experiment had much lower e.e.'s than those sampled at the end. However, the first solid rinse showed a marked improvement in e.e. for all manual solid phase samples compared with the unrinsed solids. In comparison, the second rinse showed very little change in e.e. after the initial improvement form the first rinse. Together, this data suggests that the majority of the (*R*)-**1** initially present in the solids was on the surface (mechanism ii), as a single rinse caused a drastic increase in e.e. but further rinsing showed much less change. For this reason, the "first rinse" solid phase data is plotted in Figures 8 and 9 as this data is more likely to accurately reflect the solid phase composition at each timepoint and not be impacted by surface impurities (compared with the less accurate unrinsed trends).

Despite this evidence that the majority of the (*R*)-**1** initially present in the solids was on the surface, the solids did not reach enantiopurity after rinsing, remaining at 85-90% e.e. even after two rinses. This suggests that while most of the (*R*)-**1** was crystallizing as a separate (*R*)-**1**•L-DBTA phase (i) and the majority of the (*R*)-**1** impurities in (*S*)-**1**•L-DBTA were on the crystal surface, some (*R*)-**1** was still being incorporated into the solid phase via mechanism iii or iv. The largest improvements between each rinse occurred at earlier manual samples, with little to no observable change in e.e. when the solids from the end of the experiment were rinsed. Additionally, throughout each CIDT experiment the solid phase e.e. increased slightly over time. Together, these observations suggest two possible explanations related to kinetically trapped impurities (iii):

1) (*R*)-**1** impurities are more likely to be trapped in the initial solids and that later (*S*)-**1**•L-DBTA was forming purer crystals, increasing the solid phase e.e., and/or
2) Throughout the experiment the mechanical action of the cross-shaped stir bar was grinding the solid phase and allowing kinetically trapped (*R*)-**1** to be dissolved as the crystals were milled to smaller sizes.

From the microscopic images acquired during the CIDT experiments (SI section 8), it is evident that small needle-like particles seemed to be forming and then rapidly agglomerating upon addition of L-DBTA to the solution (at t = 0 min in each experiment). This rapid agglomeration supports the idea that (*R*)-**1** impurities are initially kinetically trapped in the solid phase. Furthermore, seeding is used in Genentech's initially reported CIDT procedure to achieve e.e.'s greater than 95% for the final solids.[2] Although no time course enantiopurities are provided to indicate if the initial e.e. was this high, these higher product e.e.'s indicate that seeding upon L-DBTA addition provides more control over the purity of the solid phase and helps avoid undesired (*R*)-**1** trapping in the solid phase.

In addition to kinetically trapping (*R*)-**1**, the EasyViewer data indicates that the average particle size decreased throughout the experiments as smaller needle-like crystals crowded out larger agglomerates in the EasyViewer window. If the large agglomerates were not being broken apart throughout the experiment, it would be expected that some large agglomerates would occasionally be visible in the particle images since the particles were primarily agglomerates at the start. However, only fine particles are visible at the end of each experiment with few hints of larger masses. This suggests that both kinetic impurity hypotheses may be correct: (*R*)-**1** is indeed being kinetically trapped in the initial agglomerating particles, and mechanical grinding of the stir bar seems to be breaking apart conglomerates and purifying the solid phase. Since the final solid phase e.e. was only ~90% for each experiment, this may slightly support the former hypothesis over the latter, but also indicates that if mechanical action helps improve e.e., then increasing the forces on the crystals (by changing the stir bar geometry or introducing an additional milling step) may be a viable method of increasing the final solids' enantiopurity.

Lastly, the solution phase e.e. data from the washing experiments (Figures 25 and 27) support the above solid phase impurity hypotheses. The initial solution composition is primarily (*R*)-**1**, strongly supporting the idea that the enantiomers crystallize primarily as two separate solid phases and that (*R*)-**1**•L-DBTA is significantly more soluble than (*S*)-**1**•L-DBTA. However, subsequent rising causes the solution phase e.e. to begin to converge upon the solid phase e.e. values. This supports the conclusion that the remaining impurities are kinetically trapped and suggests that washing the final solids is not a viable method to increase product e.e. beyond a certain threshold (in this case, ~90% when no initial seeding took place).

f. Reproducing Original CIDT Procedure at Smaller Scales

Before reaction monitoring was performed on scales smaller than the originally reported CIDT procedure (50 g of *rac*-**1**),[2] this procedure was reproduced on smaller scales of 2 g, 5 g and 10 g of *rac*-**1** to confirm the validity of such small scale experiments. The results are summarized in Table SI 1. Although the resulting yields and e.e.'s are lower than the 89% yield and 95% e.e. reported by St-Jean *et al.*, the mass difference between the expected and actual solid mass is consistently ~0.8 g across all scales. This suggests that a consistent mass loss is responsible for the lower yields. Since the same filtration apparatus was used across all scale experiments, this may indicate that transfer inefficiencies during filtration were responsible for the poorer smaller scale yields. Additionally, this supports the higher 89% yield obtained by St-Jean *et al.* during their larger scale experiment with 50 g of *rac*-**1** being closest to the "true" experimental yield.

Mass *rac*-1 (g)	Expected Mass (*S*)-1• L-DBTA if 89% Yield (g)	Actual Mass (*S*)-1•L-DBTA (g)	Mass Difference from Expected 89% Yield (g)	Yield (%)	E.e. (%)
2.00	3.81	3.00	0.81	**70**	**90**
5.00	9.52	8.68	0.85	**81**	**91**
10.00	19.05	18.21	0.84	**85**	**93**

Table SI 1. Small scale replication of CIDT procedure to access (*S*)-**1**•L-DBTA reported by St-Jean *et al*.[2]

The data reported in Table SI 1 followed the reported CIDT procedure precisely, including a final EtOH wash to remove any surface impurities from the crystal surfaces before drying and analyzing their enantiopurity. Further washing of the 93% e.e. solids from the 10.0 g scale experiment was performed to determine if the enantiopurity could be improved with additional washing, and to provide further insight into the solid phase impurity incorporation. Two additional washes of 16 mL EtOH (scaled down from 80 mL EtOH in the 50 g original scale) slightly improved the e.e. from 93% to 95%. This suggests that variation in the washing procedure (temperature, volume, solvent purity, etc.) may result in enantiopurity differences in the final solids and could therefore be responsible for the varying e.e. values obtained across the tested scales. These plateauing e.e.'s of ~90-95% are also consistent with the above impurity incorporation discussion (SI section 7e), further indicating that undesired (+)-TBZ is likely on crystal surfaces or kinetically trapped between agglomerated particles and can be partially removed by washing.

Lastly, the analytical method used for chiral quantitation was not the same as that of St-Jean *et al*. We employed a reverse phase HPLC method (40% water with 10 mM NH_4OAc, 60% MeCN) using a Daicel OD-3 Chiralcel column as the stationary phase. In contrast, St-Jean *et al.* used a normal phase HPLC method (34% 2-PrOH with 0.1% $NHEt_2$, 66% *n*-Hexane) with a different chiral stationary phase (Chiralpak AD-H) with a different injection volume. High e.e. values can be drastically impacted by slight variations in the measured e.e. and require precise and accurate quantitation of the minor enantiomer. Given the differences in the analytical methods employed for e.e. quantitation, it is likely that the high e.e. values reported by St-Jean *et al.* may not correspond to precisely the same values with our instrument.

Ultimately, these variations in the yield and enantiopurity are consistent with those to be expected with reproducing an experiment across different scales with different analytical methods for quantitation. On top of this expected variation, the yield and e.e. values reported during real-time reaction monitoring experiments were further impacted by the manual and automated aliquot removal that was an integral part of real-time analysis. Together, this data supports the previously examined[5] notions that scale, procedure and analytical method differences can vastly affect reported yields and enantiopurities, serving to highlight the variation that should be expected when a result demonstrated elsewhere is attempted to be replicated.

8. Particle Images (EasyViewer Data)

a. Images from CIDT Experiment (Chiral) – Figures 2 and 9

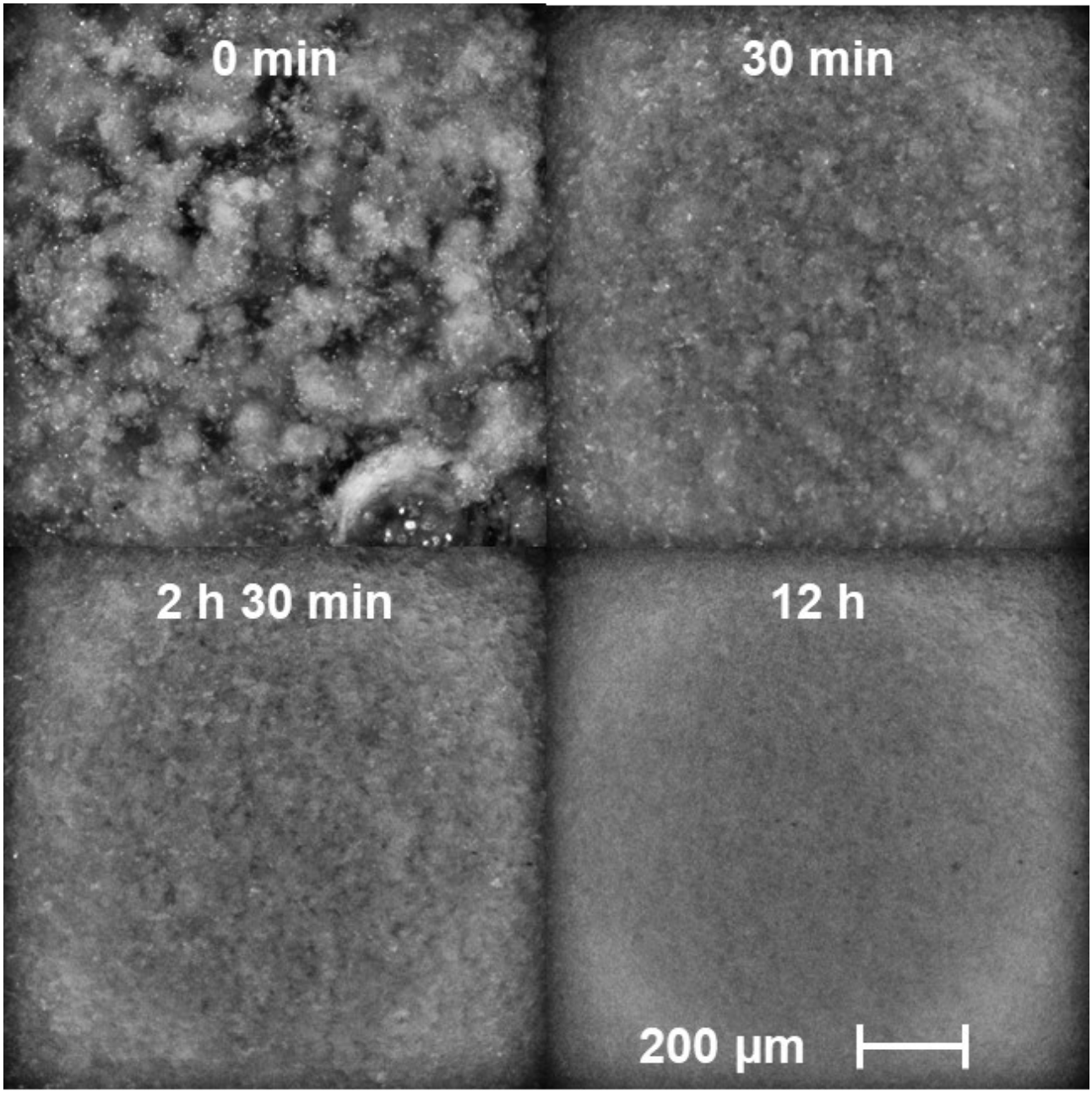

Figure SI 29. Microscopic images of crystals from CIDT experiment monitored *via* chiral online HPLC, illustrating initial formation of large crystallite agglomerates (at 0 min) and formation of very fine crystals pressing against the window that begin to obscure the large agglomerates (by 30 min) and eventually are all that is visible (by 12 h).

b. Images from CIDT Experiment (Achiral) – Figures 3 and 8

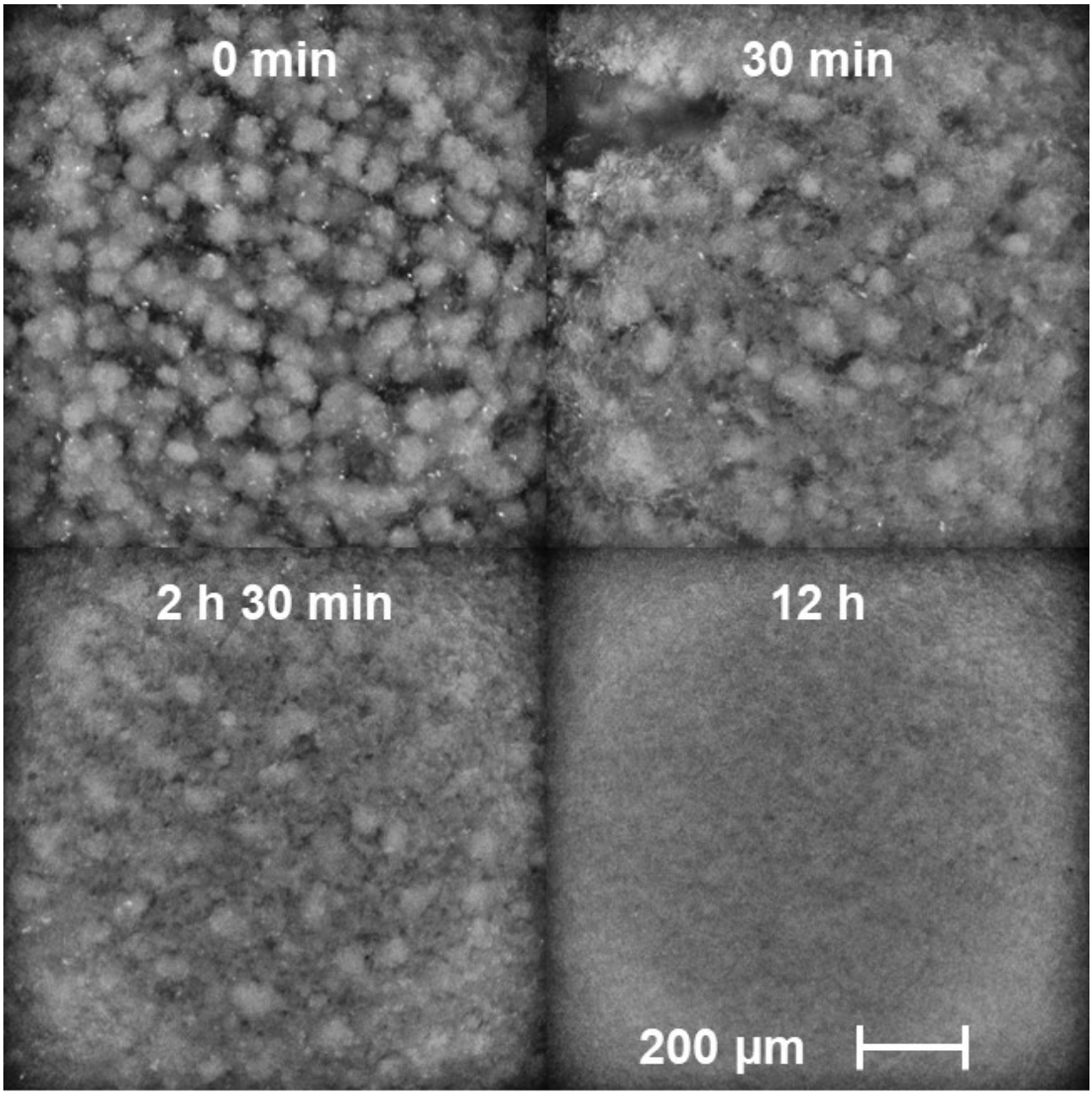

Figure SI 30. Microscopic images of crystals from CIDT experiment monitored *via* achiral online HPLC, illustrating initial formation of large crystallite agglomerates (at 0 min) and formation of very fine crystals pressing against the window that begin to obscure the large agglomerates (by 30 min) and eventually are all that is visible (by 12 h).

c. Images from CIDT with L-DBTA Undercharge – Figure 4

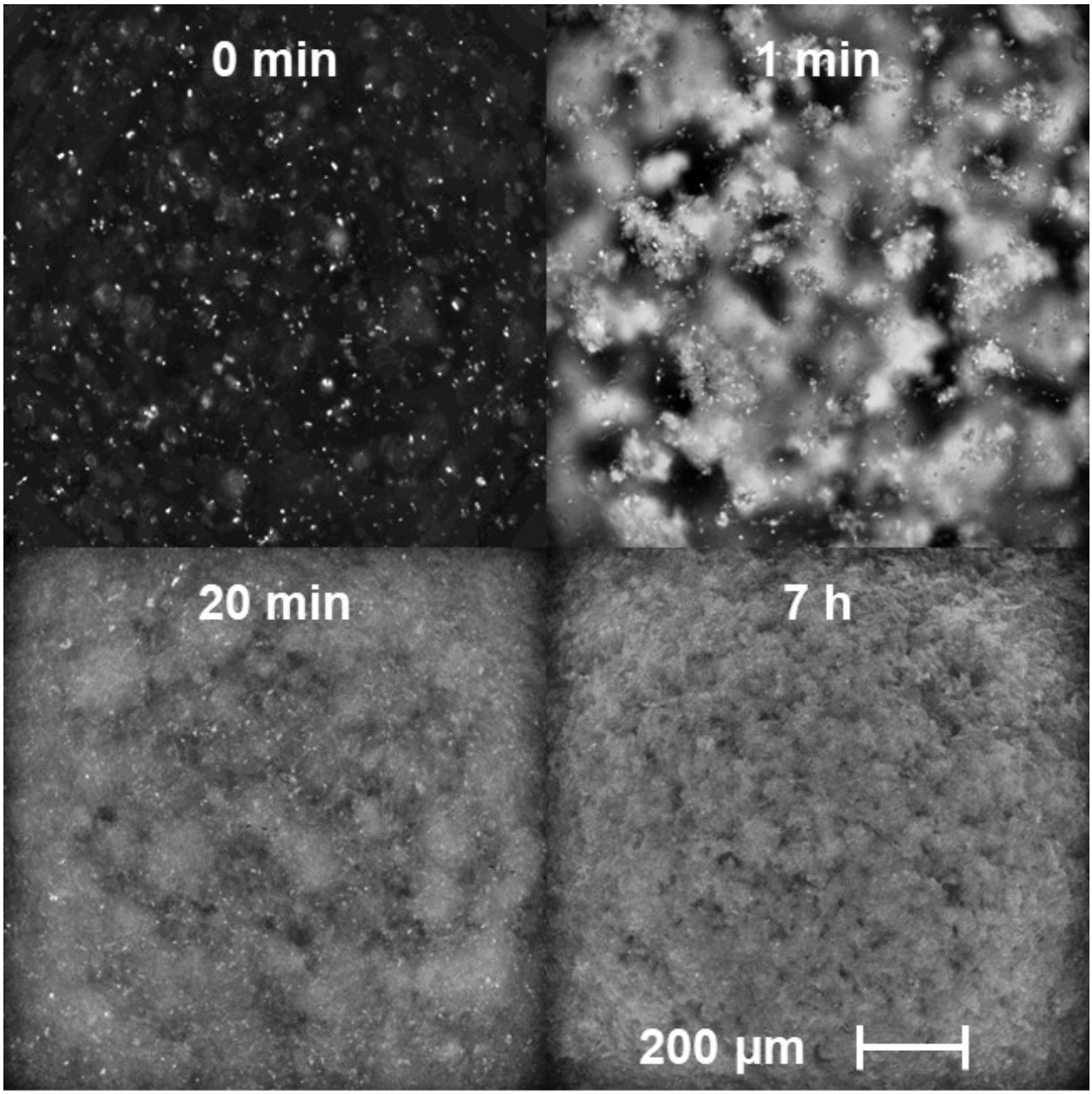

Figure SI 31. Microscopic images of crystals from CIDT experiment with L-DBTA undercharge (0.9 equiv), illustrating formation of small needle-like crystals at 0 min (time of L-DBTA dosing), rapid crystallite agglomeration (at 1 min), formation of a film over the viewer screen by 20 min (obscuring most images after this point), and formation of very fine crystals pressing against the window by 7 h that brought the solution back into focus.

9. Optimizing Inline Racemization

a. Procedure

Optimal racemization conditions were desired to recover more (S)-1•L-DBTA from the end solution phase of a CIDT experiment such as Figures 2 and 3. As such, a saturated solution of (*R*)-**1**•L-DBTA and (*S*)-**1**•L-DBTA at 20 °C was prepared in order to optimize inline racemization with a solution as close as possible to the composition at the end of CIDT experiment at 20 °C, with added L-DBTA since excess L-DBTA (1.4 equiv) was used. *Rac*-**1** (1.81 g, 5.76 mmol) and L-DBTA (2.17 g, 5.76 mmol, 1.0 equiv) were therefore added to 120 mL of EtOH in a 100 mL EasyMax flask stirring at 20 °C. After being left overnight, a white solid formed and was isolated by suction filtration (1.32 g, 81 % e.e. of (*S*)-**1**•L-DBTA). The amount of (*R*)-**1**•L-DBTA and (*S*)-**1**•L-DBTA remaining in the filtrate was then calculated, and the e.e. verified by sampling the solution phase (consistently ~60% e.e. of (*R*)-**1**•L-DBTA as that salt of **1** is more soluble). The solution was then passed through the inline racemization chamber and backpressure regulator and collected afterward for e.e. analysis. Once the effluent e.e. was known, the amount of each enantiomer of **1** could be calculated based on the initial concentration of the solution (determined from the mass of the isolated solid phase). This was then used to determine the optimal racemization conditions.

b. Theory and Calculations

From our initial racemization experiments (SI section 7d), it was evident that higher temperatures and the presence of L-DBTA were beneficial for the racemization of (*S*)-**1** into *rac*-**1**. A backpressure regulator (BPR) was therefore incorporated into our flow system to allow temperatures above the boiling point of EtOH to be tested. Altogether, the effects of temperature, flow rate (*i.e.,* residence time) and equivalence of L-DBTA (*i.e.,* L-DBTA concentration) were investigated on solutions prepared according to the above procedure. Having no easy way to measure the temperature of the solution being passed through the racemizer (since the solution was pressurized and could therefore be heated above its boiling point thanks to the BPR), the temperature of the jacket of the thermostat unit (T_j) was controlled instead of using the typical reactor temperature (T_r) control of the other experiments. Aluminum beads were placed inside the resin racemization coil to help increase its heat capacity and ensure more even heating (Figure SI 2). However, given that the tubing was made of ETFE and the racemization chamber made of resin, the heat transfer capabilities of our system were not ideal and the actual solution temperature was likely below that of the jacket (T_j) in all cases. Our study therefore focused on finding the optimal conditions for our setup (and not engineering an ideal flow system) to demonstrate our proof of concept that inline racemization could be used to improve a CIDT.

If a set residence time was always being used, the optimal inline racemization conditions could be determined simply by analyzing the effluent solution and determining the temperature and concentration of L-DBTA that provide the largest change in concentration of (*R*)-**1** into (*S*)-**1**. However, we instead needed a method of incorporating the changes in process efficiency that would occur as flow rate was varied (since a slower flow rate may result in more racemization but would conversely take longer to turn over (*R*)-**1** into (*S*)-**1**). As such, we first calculated the change in (*R*)-**1** concentration (Δ[(*R*)-**1**], in M) that occurred after passing the solution through the inline racemization chamber for residence time (t):

$$\Delta[(R)-1]\,(M) = \Delta[(R)-1]_{0} - \Delta[(R)-1]_{t} \quad \text{Eqn 1}$$

This change in (*R*)-**1** concentration could then be converted into a change in mmol of (*R*)-**1** by multiplying by the racemization coil volume (5.1 mL), and then converted further into an absolute rate of racemization (Δmmol/h) by dividing by the residence time of the solution (in h):

$$Rate\ of\ Racemizaiton\ (\Delta mmol/h) = \frac{\Delta[(R)-1]\,(M) \times Coil\ Volume\ (mL)}{Residence\ Time\ (h)} \quad \text{Eqn 2}$$

Finally, the total excess amount of (*R*)-**1** calculated to be present in solution at the end of the CIDT experiments (*i.e.,* the total amount of (*R*)-**1** that could be racemized into *rac*-**1**, $mmol_{tot}$) was then divided by this absolute rate of racemization (Δmmol/h) to afford the total process time (T_{tot}, in h) that a solution would require in order to be fully racemized with a specific set of inline racemization conditions:

$$T_{tot}\,(h) = \frac{mmol_{tot}}{Rate\ of\ Racemization\ (\Delta mmol/h)} \quad \text{Eqn 3}$$

From the earlier CIDT experiments, the total excess amount of (*R*)-**1** still in solution after performing the CIDT ($mmol_{tot}$) seemed to be roughly 5.53 mmol. As such, this value was used with Eqn 3 to calculate the total process time (T_{tot}) for all tested inline racemization conditions after determining the solution e.e. from effluent analysis (*via* offline chiral HPLC) and converting the e.e. data to enantiomer solution concentrations for use in Eqn 1 and Eqn 2.

c. Testing Effect of L-DBTA Concentration and Residence Time at T_j = 85 °C

0.0315 M solution of (*R*)-**1** and (*S*)-**1** (59% e.e. towards (*R*)-**1**) in EtOH containing 0.0378 M L-DBTA was passed through the inline racemization coil while the jacket temperature (T_j) was maintained at 85 °C. Two different flow rates were used to achieve residence times of 2.55 and 25.5 min, the effluent exiting the BPR was collected, and the total process times calculated. Additional L-DBTA was added to the remaining starting solution and the procedure repeated with L-DBTA concentrations of 0.063 M, 0.110 M and 0.158 M (Figure SI 32).

Despite more racemization being observed using the longer residence time, Figure SI 32 shows that this also resulted in significantly longer total process times (170-290 h) than the shorter residence time of 2.55 min for all L-DBTA concentrations (~50 h). This suggested that although a longer residence time gives the solution more time to heat, the slower flow rate detracts from the viability of such long residence times. Additionally, increasing the concentration of L-DBTA from 0.0378 M to 0.158 M resulted in a slight decrease in total process time from 63 h to 44 h, suggesting that higher L-DBTA concentrations may increase the rate of racemization. However, given the relatively small effect observed from changing the L-DBTA concentration from 0.0378 M to over four times this value at 0.158 M, and the observation that the solution exiting the BPR was not boiling, higher temperatures were next investigated to hopefully speed up racemization.

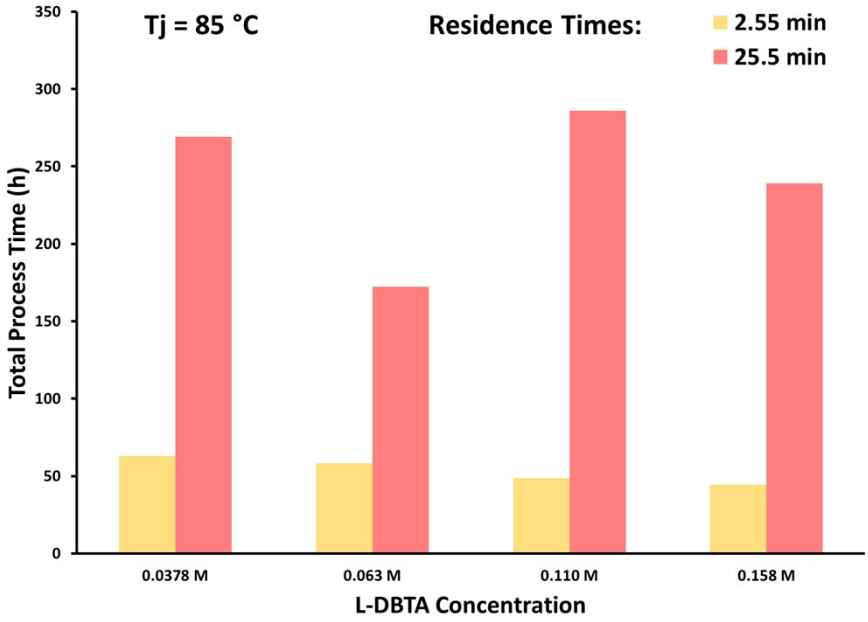

Figure SI 32. Total process times for 0.0315 M solution of (*R*)-**1** and (*S*)-**1** (59% e.e. towards (*R*)-**1**) in EtOH passed through the racemization coil (T_j = 85 °C) at residence times of 2.55 and 25.5 min, for four different concentrations of L-DBTA.

d. Testing Effect of Temperature and Residence Time

0.032 M solution of (*R*)-**1** and (*S*)-**1** (59% e.e. towards (*R*)-**1**) in EtOH containing 0.032 M L-DBTA was passed through the inline racemization coil while the jacket temperature (T_j) was maintained at 85, 110 °C. Three different flow rates were used to achieve residence times of 2.55 and 25.5 min, the effluent exiting the BPR was collected, and the total process times calculated. The procedure was repeated with 0.027 M solution of (*R*)-**1** and (*S*)-**1** (59% e.e. towards (*R*)-**1**) in EtOH containing 0.027 M L-DBTA once it was determined that T_j = 140 °C gave shorter total process times than 85 °C or 110 °C. An additional residence time of 5.10 min was screened to narrow down the optimal conditions further (Figure SI 33).

Higher temperatures and longer residence times gave shorter total process times overall, although significant degradation of **1** was observed at 140 °C with a 25.5 min residence time. The lowest total process time was calculated to result from a jacket temperature of 130 °C with a 5.10 min residence time (between the previously tested residence times of 2.55 and 25.5 min). Additionally, significantly less degradation was observed at T_j = 130 °C compared with 140 °C. This suggests that balancing higher temperatures (to achieve racemization, given the poor heat transfer of our system) with medium residence times (to avoid decomposition with extended heating) is key to minimizing the total process time and avoiding undesired decomposition while maximizing racemization. As such, a jacket temperature of 130 °C was selected for further optimization of residence time and L-DBTA concentration.

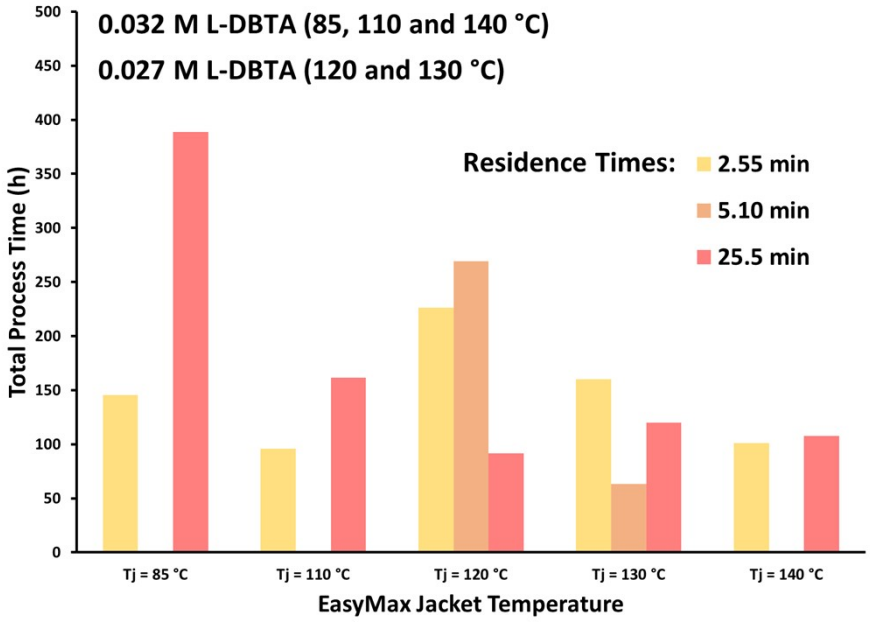

Figure SI 33. Total process times for 0.032 M (T_j = 85, 110 and 140 °C) and 0.027 M (T_j = 120 and 130 °C) solution of (*R*)-**1** and (*S*)-**1** (59% e.e. towards (*R*)-**1**) in EtOH passed through the racemization coil at residence times of 2.55 (5.10) and 25.5 min at different temperatures.

e. Testing Effect of L-DBTA Concentration and Residence Time at T_j = 130 °C

0.027 M solution of (*R*)-**1** and (*S*)-**1** (59% e.e. towards (*R*)-**1**) in EtOH containing 0.027 M L-DBTA was passed through the inline racemization coil while the jacket temperature (T_j) was maintained at 130 °C. Three different flow rates were used to achieve residence times of 2.55, 5.10 and 25.5 min, the effluent exiting the BPR was collected, and the total process times calculated. Additional L-DBTA was added to the remaining starting solution and the procedure repeated with an L-DBTA concentration of 0.054 M, (Figure SI 34).

The lowest total process times were calculated to occur with residence times of 5.10 min for both concentrations of L-DBTA, with the higher concentration (0.054 M) showing a slightly lower total process time (46 h) than the lower concentration (63 h). To further optimize our inline racemization conditions, the experiment was therefore repeated with intermediate residence times longer than 5.10 min but shorter than 25.5 min.

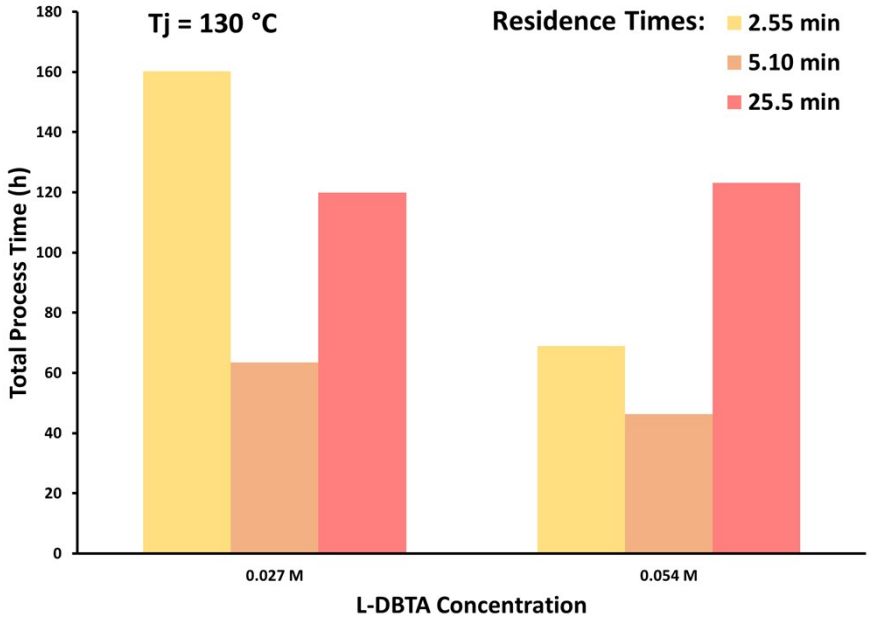

Figure SI 34. Total process times for 0.027 M solution of (*R*)-**1** and (*S*)-**1** (59% e.e. towards (*R*)-**1**) in EtOH passed through the racemization coil (T_j = 130 °C) at residence times of 2.55, 5.10 and 25.5 min for two different concentrations of L-DBTA.

Repeating the experiment at T_j = 130 °C with 0.028 M solution of (*R*)-**1** and (*S*)-**1** (59% e.e. towards (*R*)-**1**) in EtOH containing 0.028 M L-DBTA, residence times of 6.38, 8.5, 12.75 and 25.5 min were tested and additional L-DBTA was added to test a concentration of 0.056 M L-DBTA (Figure SI 35). Of these, the lowest total process time yet of 23 h was calculated for both concentrations of L-DBTA. However, with these residence times longer than 5.10 min, the pumping of the solution was observed to be slow enough that the effluent was leaving the BPR at an inconsistent rate (in spurts, rather than consistently). As such, despite the lower total process times provided by these intermediary residence times, the optimal inline racemization conditions for our racemization coil were determined to be T_j = 130 °C with a residence time of 5.10 min. This temperature and residence time were therefore used in the inline racemization experiments presented in the main text

L-DBTA concentration did not play a major role in the racemization, as expected if it is acting as a general acid catalyst to promote racemization via conjugated intermediate **2**. The same total process time (23 h) was observed for both 0.028 M and 0.056 M (*i.e.,* 1.0 and 2.0 equiv L-DBTA) at 130 °C. Additionally, the amount of L-DBTA present after a CIDT experiment would depend on both the degree of (*S*)-**1**•L-DBTA crystallization and L-DBTA decomposition. As such, the concentration of L-DBTA was determined to be difficult to control after a crystallization, and the presence of excess L-DBTA (1.4 equiv according to the original CIDT procedure[2]) was determined to be sufficient for inline racemization without the need for further optimization.

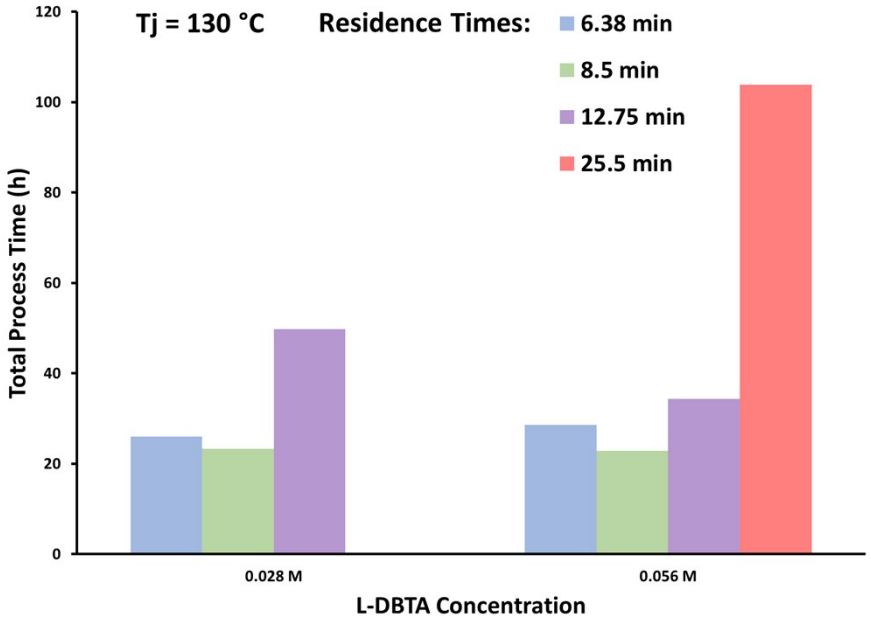

Figure SI 35. Total process times for 0.028 M solution of (*R*)-**1** and (*S*)-**1** (59% e.e. towards (*R*)-**1**) in EtOH passed through the racemization coil (T_j = 130 °C) at residence times of 6.38, 8.5, 12.75 and 25.5 min for two different concentrations of L-DBTA.

10. PXRD Data

a. *rac*-**1**

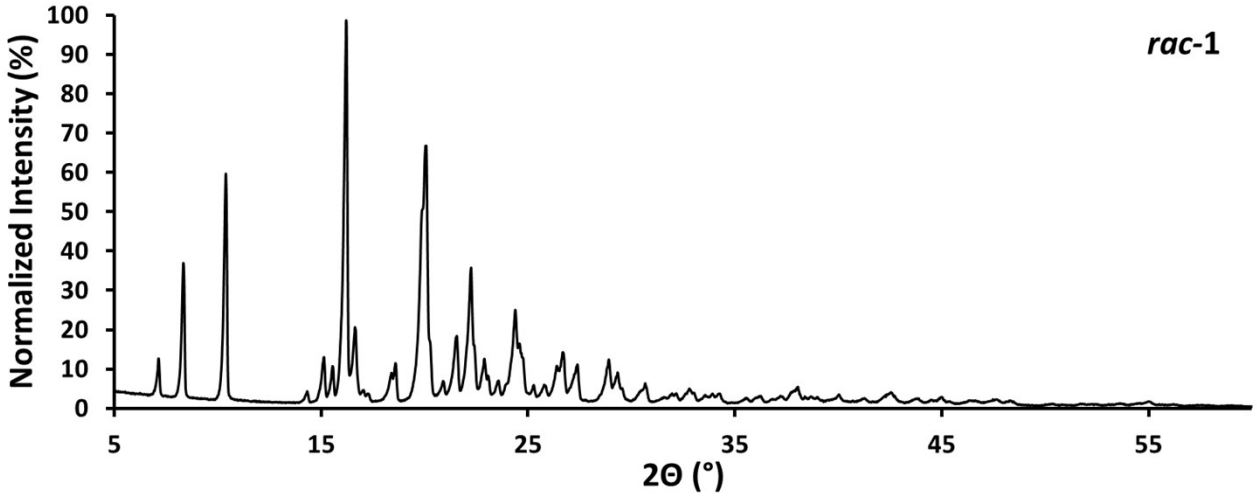

Figure SI 36. PXRD pattern for *rac*-**1** isolated from EtOH.

b. (*S*)-**1**•L-DBTA

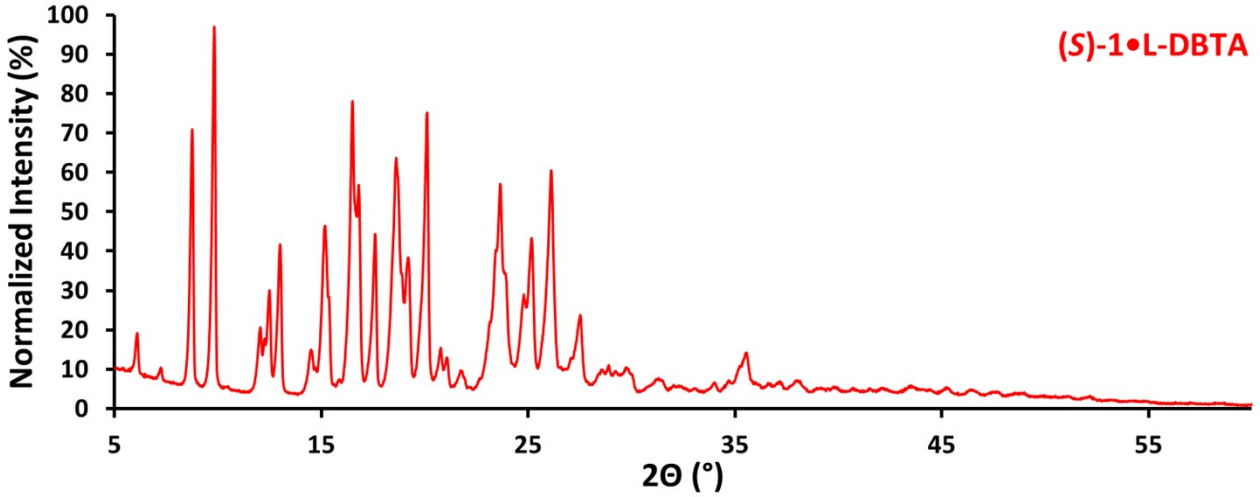

Figure SI 37. PXRD pattern for 90% e.e. (*S*)-**1**•L-DBTA isolated from the reported CIDT procedure.[2]

c. Mixture of (*R*)-**1**•L-DBTA and (*S*)-**1**•L-DBTA

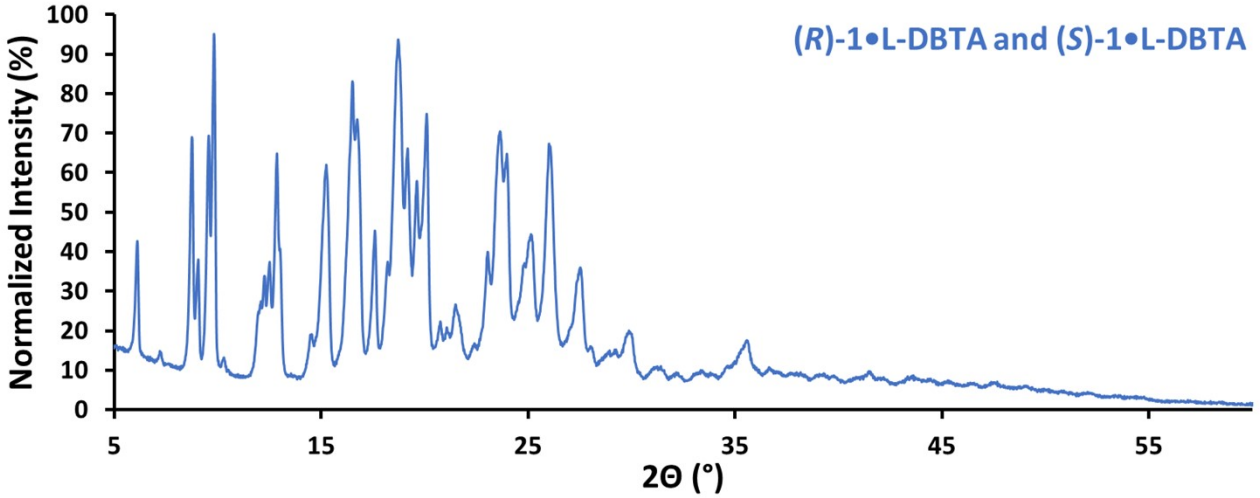

Figure SI 38. PXRD pattern for a mixture of (*R*)-**1**•L-DBTA and (*S*)-**1**•L-DBTA isolated from EtOH.

d. Comparison of (*S*)-**1**•L-DBTA and Mixture of (*R*)-**1**•L-DBTA and (*S*)-**1**•L-DBTA

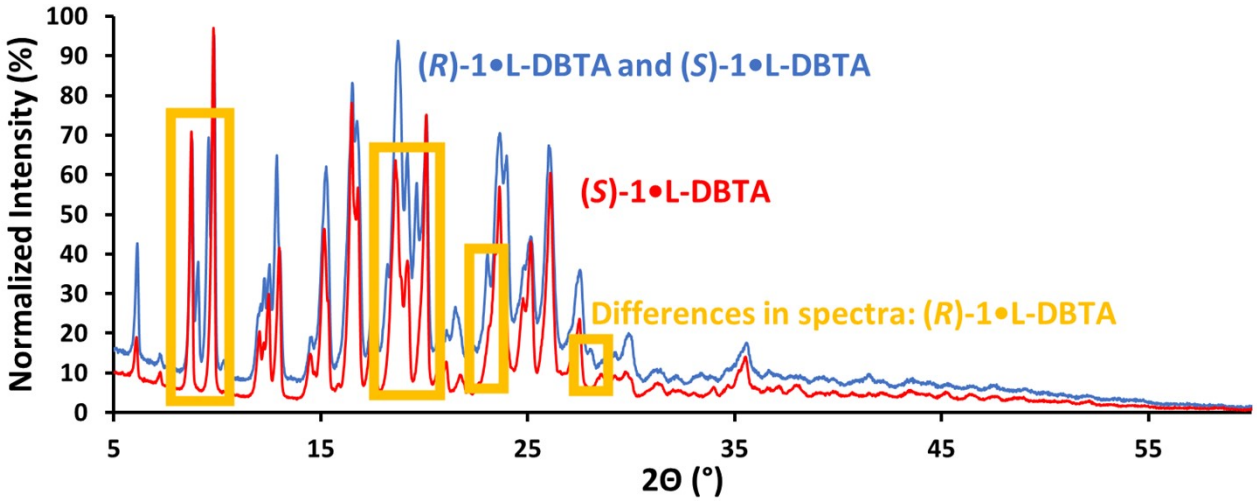

Figure SI 39. Comparison of PXRD patterns for 90% e.e. (*S*)-**1**•L-DBTA and a mixture of (*R*)-**1**•L-DBTA and (*S*)-**1**•L-DBTA, highlighting key differences suggesting that (*R*)-**1**•L-DBTA and (*S*)-**1**•L-DBTA form separate crystal phases (since all (*S*)-**1**•L-DBTA peaks are present in the mixture).

11. NMR Data

a. Desired Epimer: Compound **1** (trans cyclohexanol configuration)

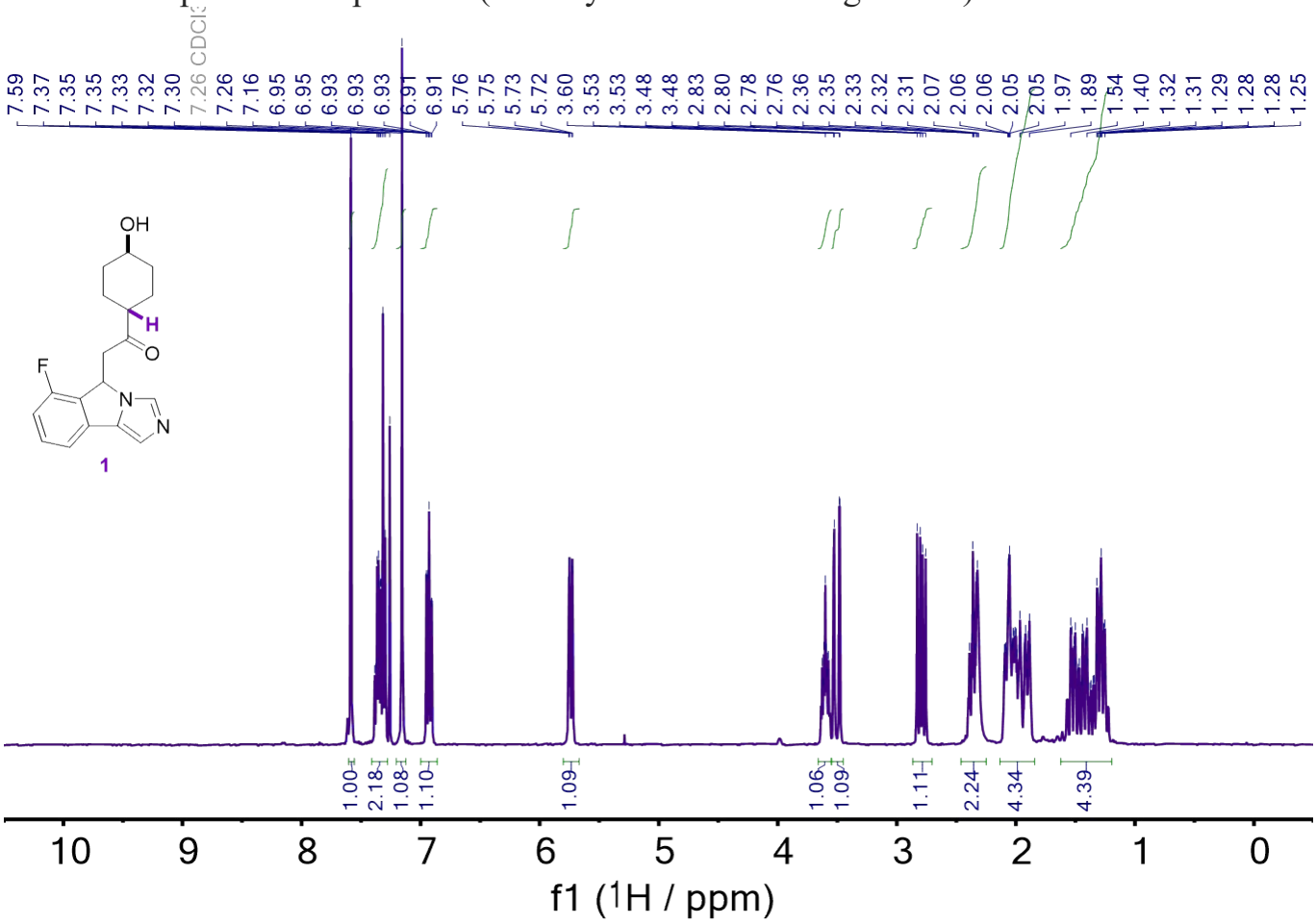

Figure SI 40. ^{1}H NMR ($CDCl_3$, 400 MHz) spectrum of compound **1**.

^{1}H NMR ($CDCl_3$, 400 MHz): δ 7.59 (s, 1H), 7.41 – 7.24 (m, 2H), 7.16 (s, 1H), 6.93 (ddd, 1H, *J* = 9.5, 8.0, 1.1 Hz), 5.74 (dd, 1H, *J* = 10.6, 2.4 Hz), 3.60 (tt, 1H, *J* = 10.7, 4.3 Hz), 3.51 (dd, 1H, *J* = 18.6, 2.2 Hz), 2.79 (dd, 1H, *J* = 18.6, 10.6 Hz), 2.45 – 2.22 (m, 2H), 2.14 – 1.79 (m, 4H), 1.59 – 1.20 (m, 4H).

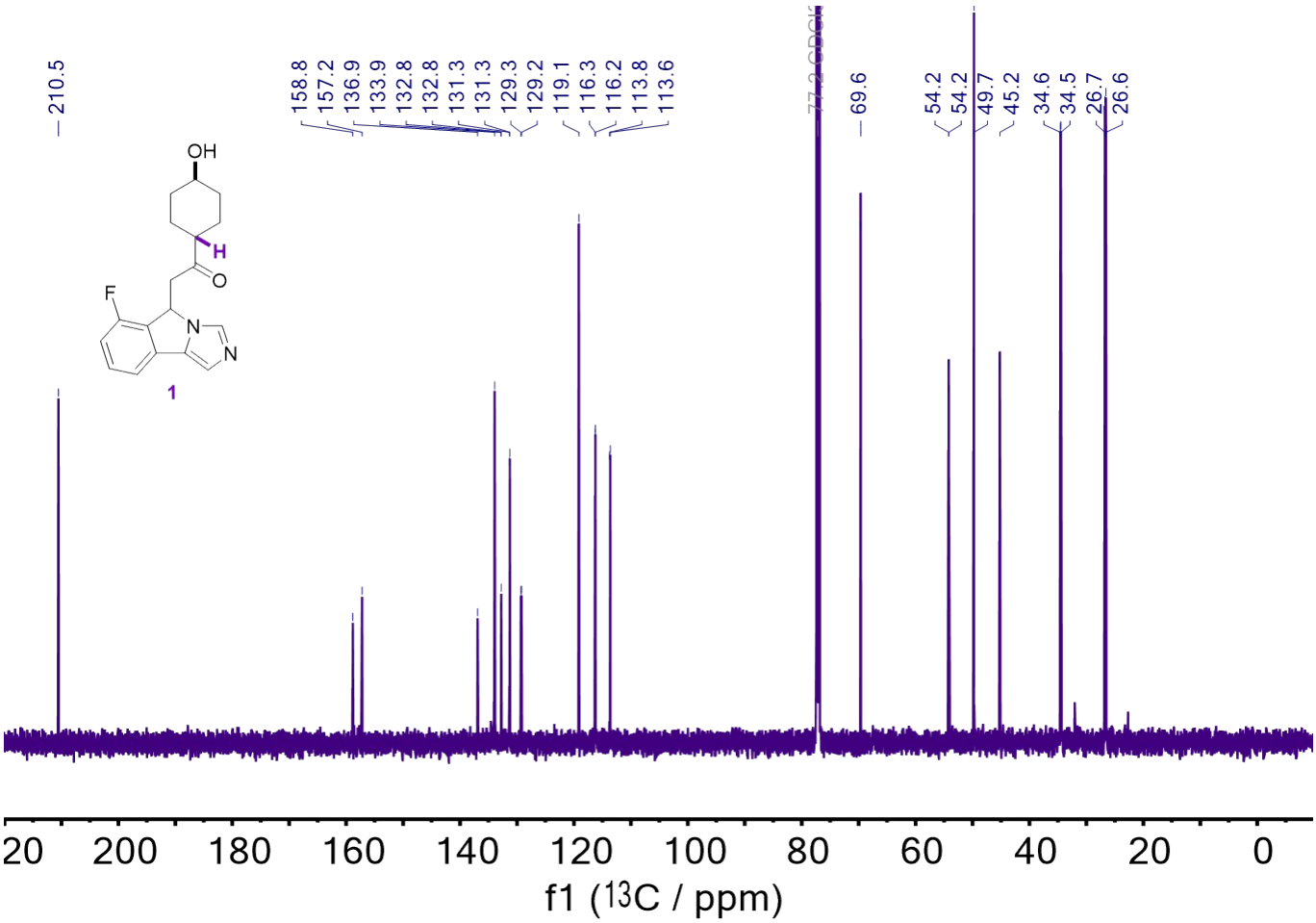

Figure SI 41. ^{13}C NMR ($CDCl_3$, 151 MHz) spectrum of compound **1**.

^{13}C NMR ($CDCl_3$, 151 MHz): δ 210.5, 158.0 (J_{CF} = 247 Hz), 136.9, 133.9, 132.8 (J_{CF} = 6.2 Hz), 131.3 (J_{CF} = 8.4 Hz), 129.3 (J_{CF} = 16.0 Hz), 119.1, 116.3 (J_{CF} = 3.5 Hz), 113.7 (J_{CF} = 20.0 Hz), 69.6, 54.2 (J_{CF} = 1.4 Hz), 49.7, 45.2, 34.6, 34.5, 26.7, 26.6.

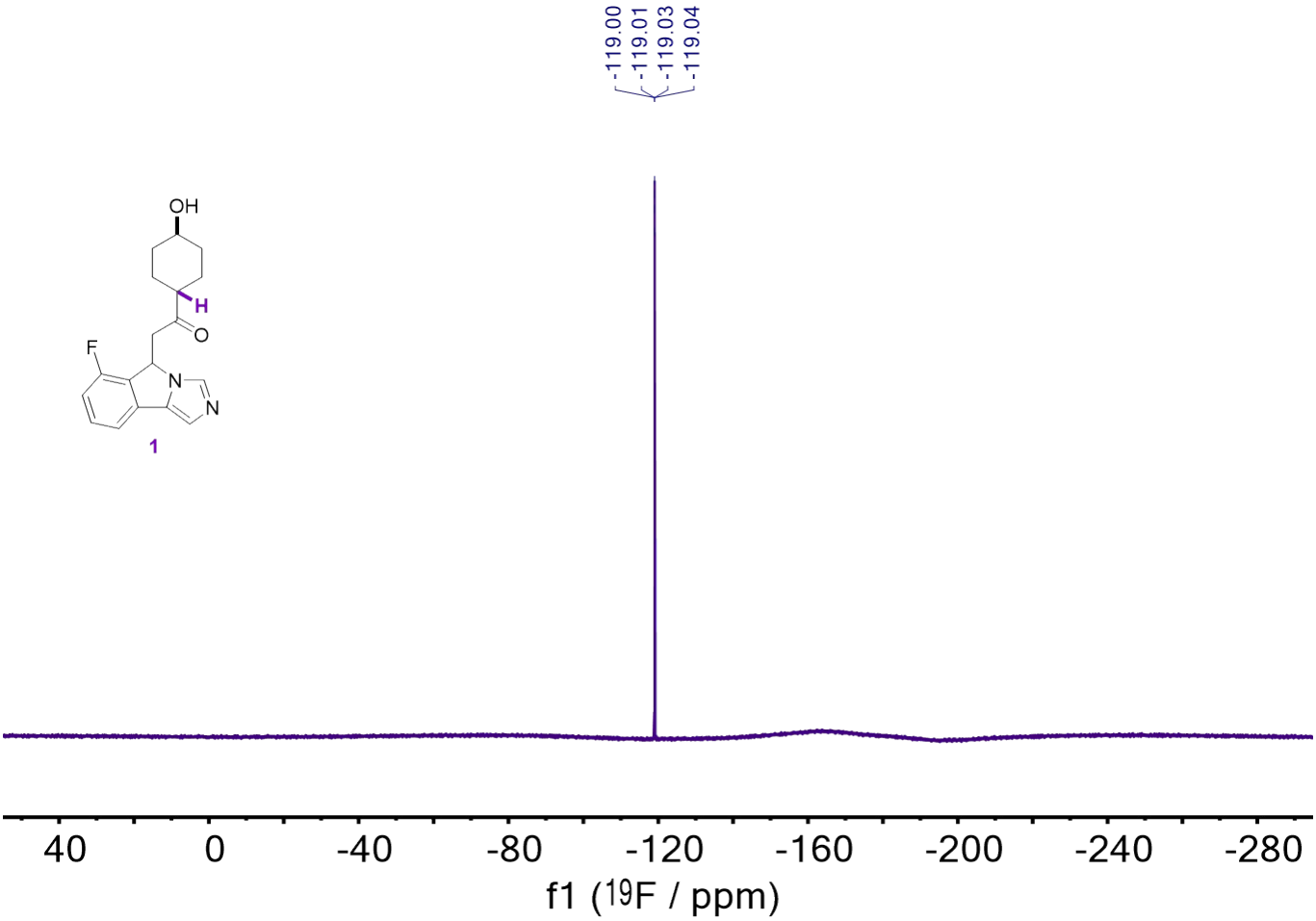

Figure SI 42. ^{19}F NMR ($CDCl_3$, 376 MHz) spectrum of compound **1**.

^{19}F NMR ($CDCl_3$, 376 MHz): δ -119.0 (dd, $J_{F,H}$ = 10.0, 4.9 Hz).

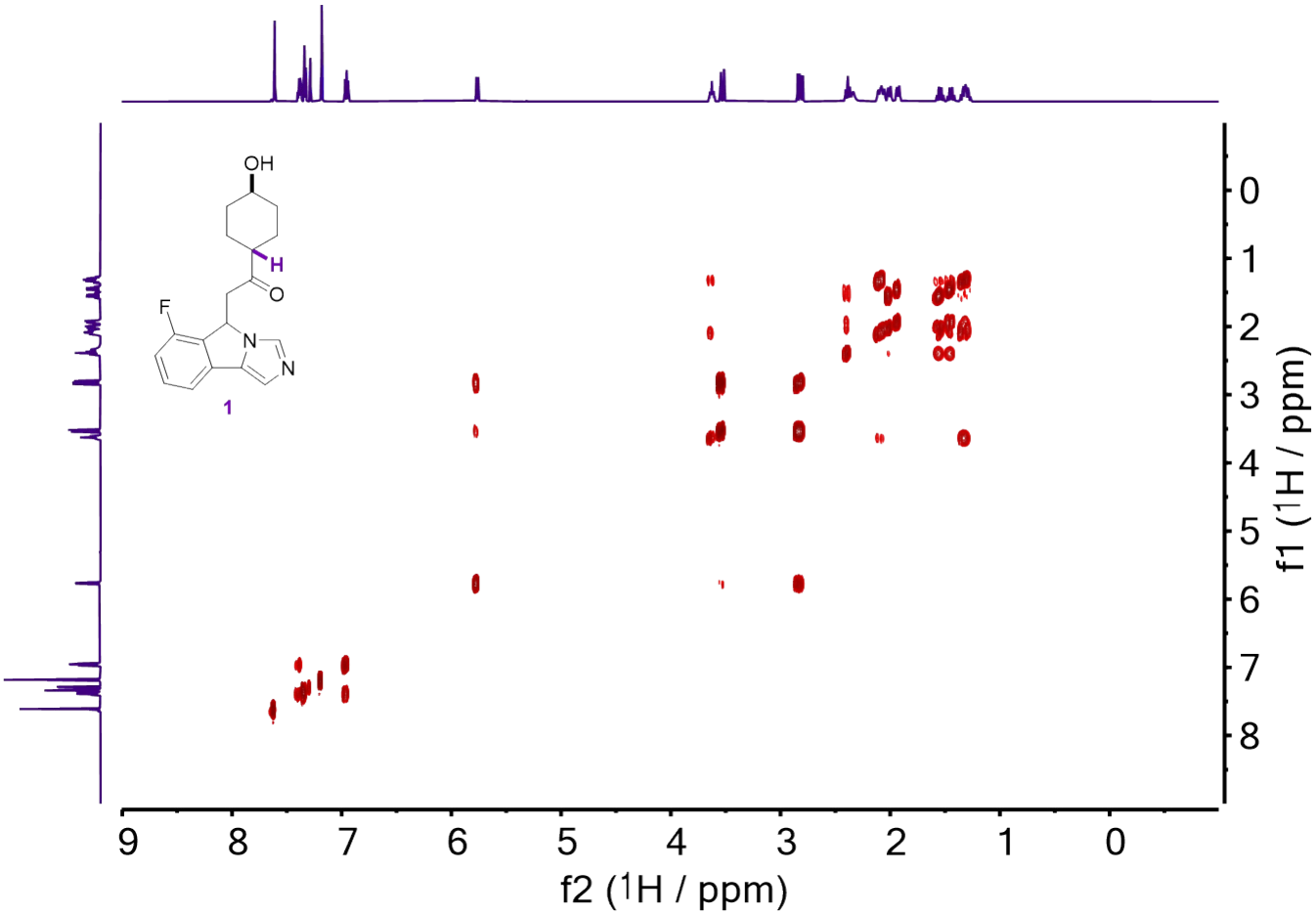

Figure SI 43. COSY NMR ($CDCl_3$, 600 MHz) spectrum of compound **1**.

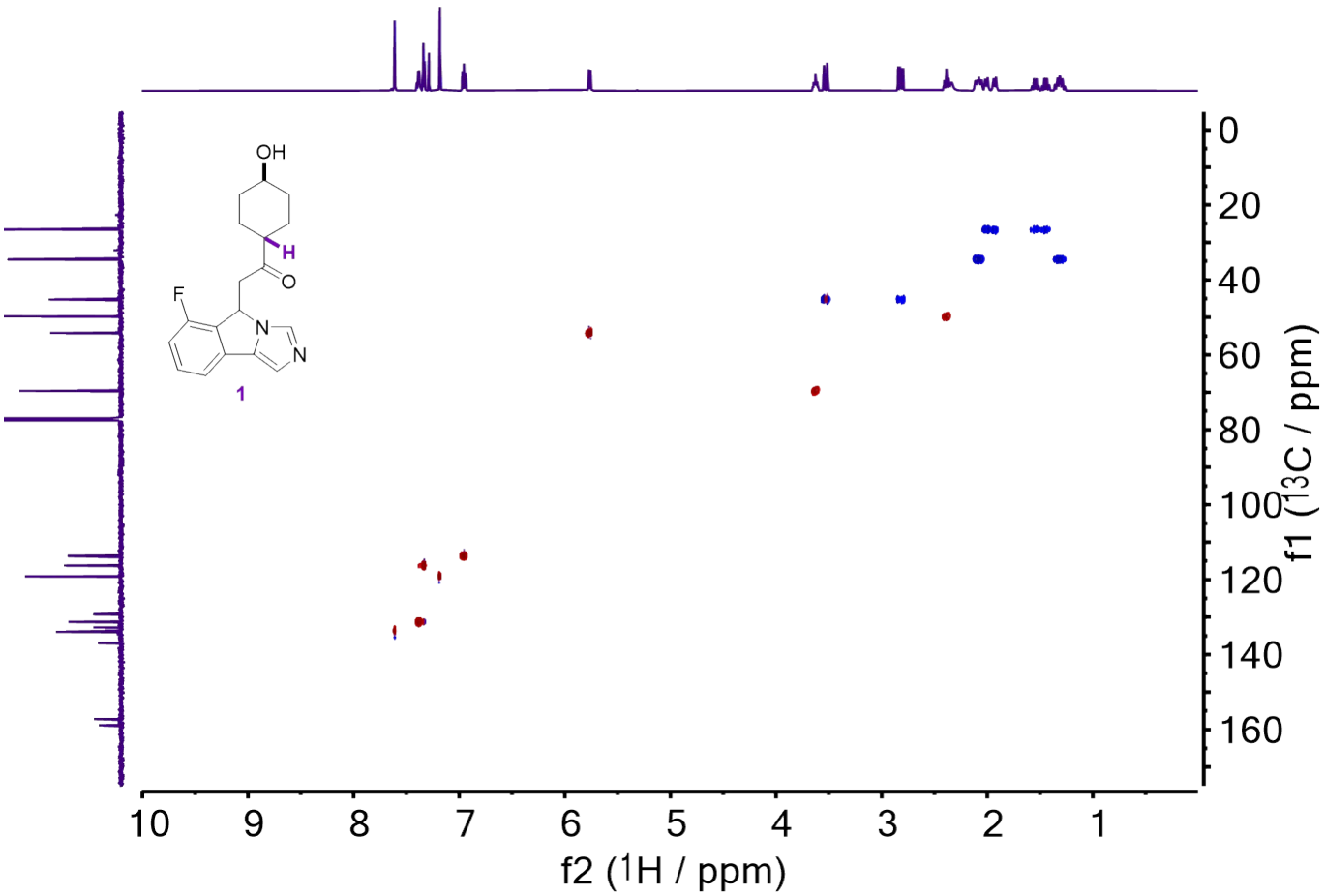

Figure SI 44. HSQC NMR ($CDCl_3$, ^{1}H: 600 MHz, ^{13}C: 151 MHz) spectrum of compound **1**.

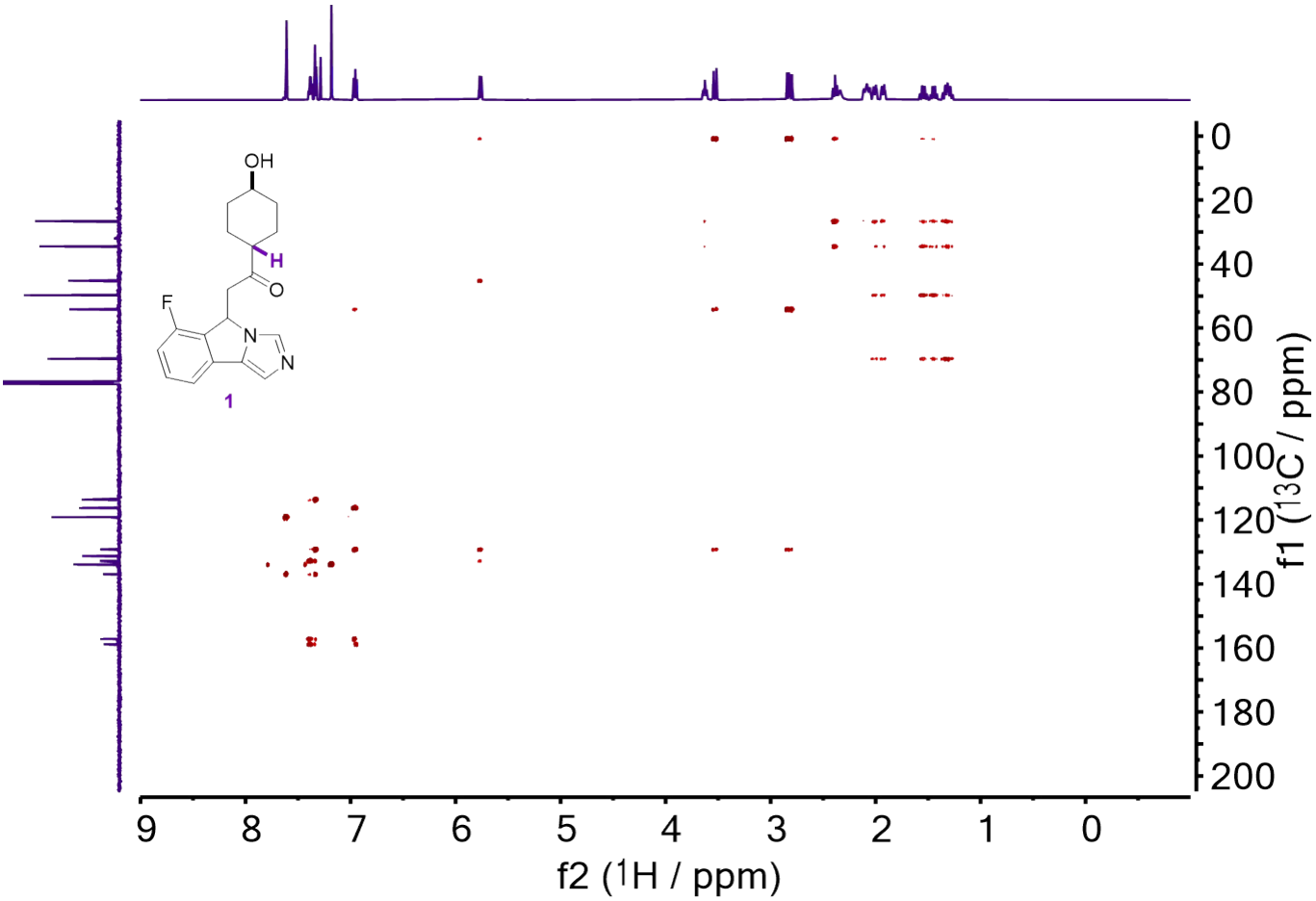

Figure SI 45. HMBC NMR ($CDCl_3$, ^{1}H: 600 MHz, ^{13}C: 151 MHz) spectrum of compound **1**.

b. Undesired Epimer: Compound **3**

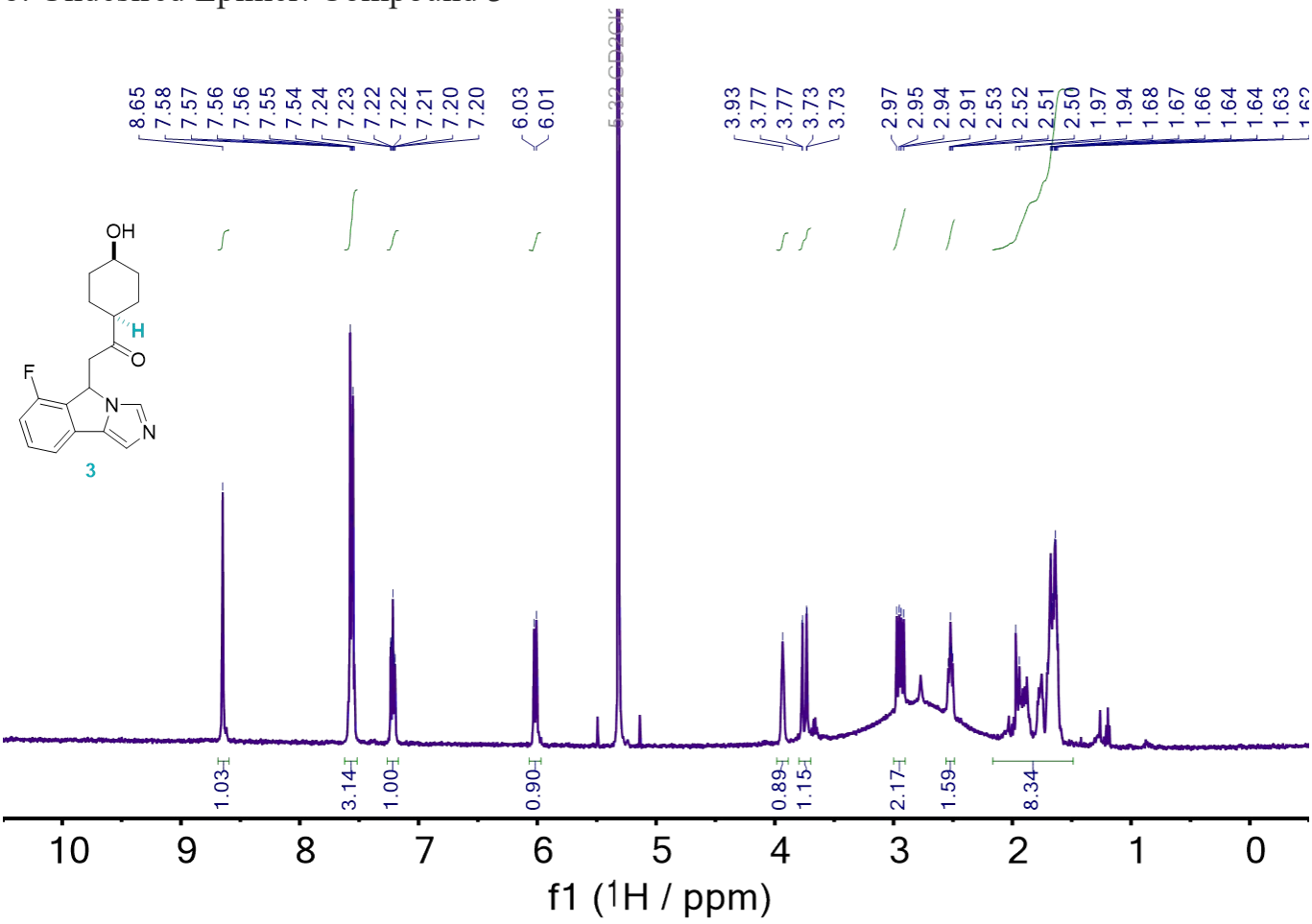

Figure SI 46. ^{1}H NMR (CD_2Cl_2, 500 MHz) spectrum of compound **3**.

^{1}H NMR ($CDCl_3$, 500 MHz): δ 8.65 (s, 1H), 7.61 – 7.52 (m, 3H), 7.22 (ddd, 1H, J = 9.4, 7.2, 1.9 Hz), 6.02 (d, 1H, J = 10.5 Hz), 3.93 (s, 1H), 3.77 (d, 1H, J = 2.0 Hz), 2.94 (dd, 1H, J = 19.0, 10.7 Hz), 2.56 – 2.48 (m, 1H), 1.95 – 1.86 (m, 2H), 1.81 – 1.74 (m, 1H), 1.73 – 1.60 (m, 5H).

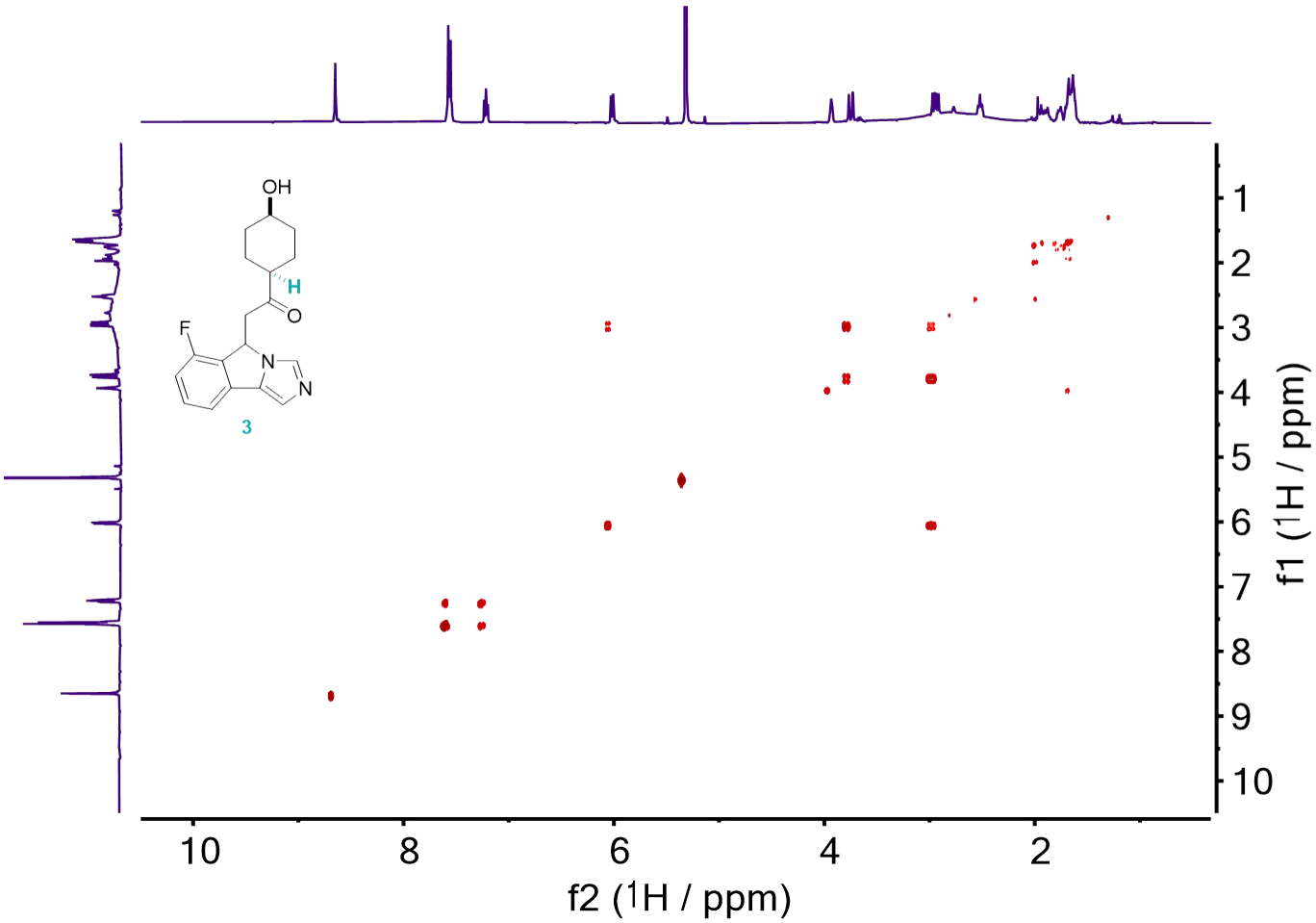

Figure SI 47. COSY NMR (CD_2Cl_2, 500 MHz) spectrum of compound **3**.

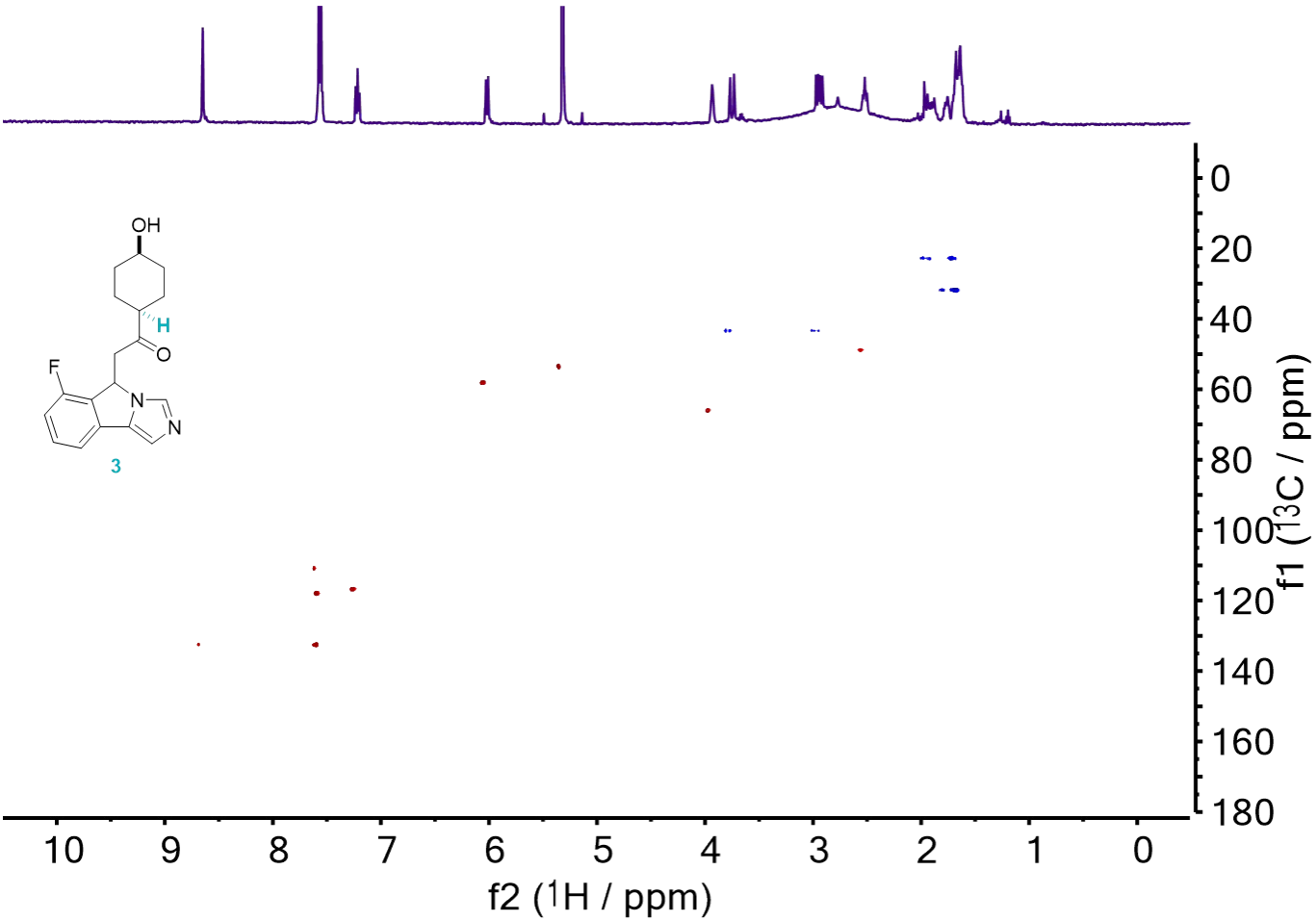

Figure SI 48. HSQC NMR (CD_2Cl_2, ^{1}H: 500 MHz, ^{13}C: 126 MHz) spectrum of compound **3**.

c. HSQC Comparison Between Epimers: Compounds **1** (trans) and **3** (cis)

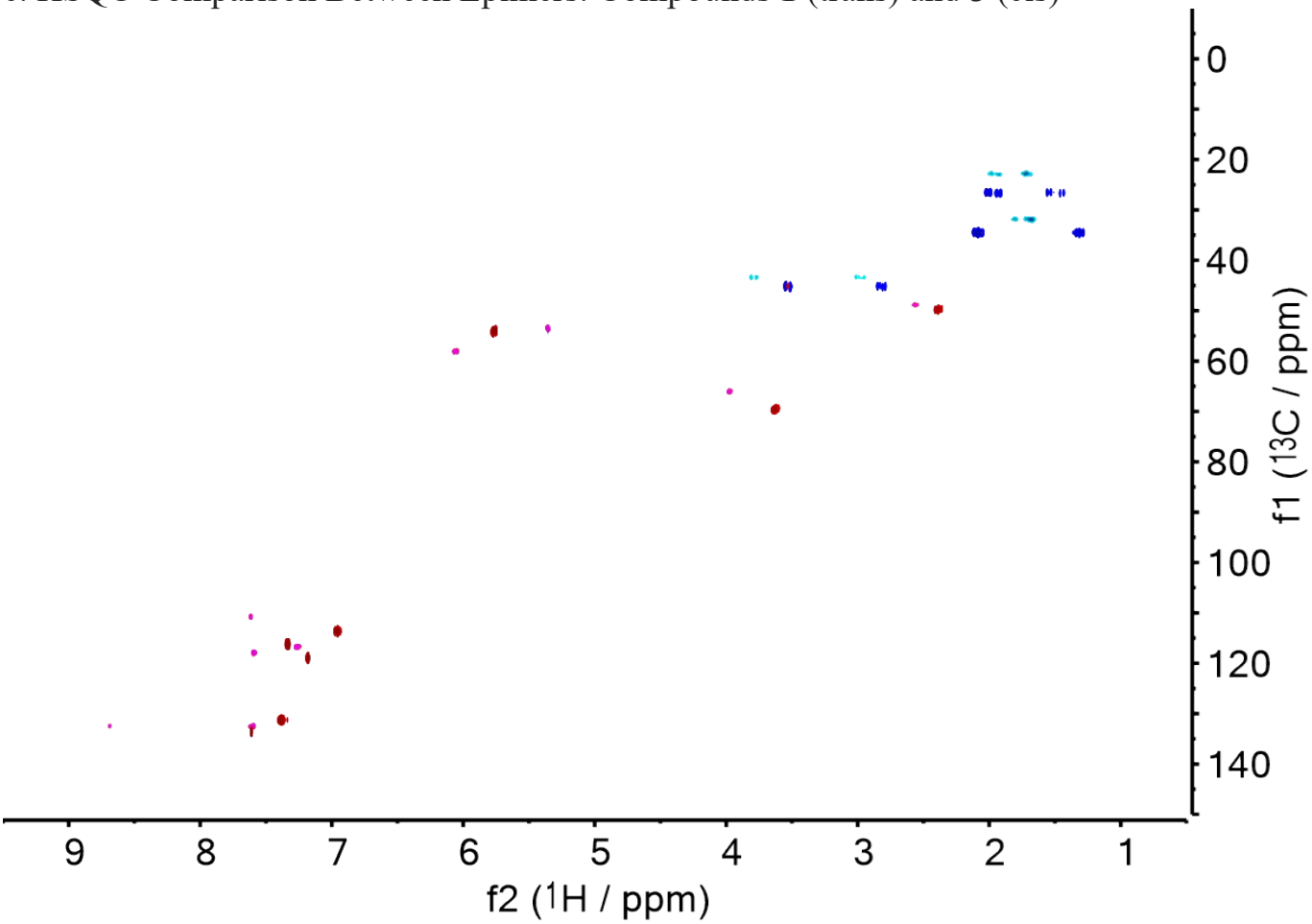

Figure SI 49. HSQC NMR comparison between compound **1** ($CDCl_3$, ^1H: 600 MHz, ^{13}C: 151 MHz) and compound **3** (CD_2Cl_2, ^1H: 500 MHz, ^{13}C: 126 MHz), with compound **1** darker and compound **3** lighter. Shifted resonances are proposed to be due to cyclohexanol epimers resting in different configurations, changing the chemical shifts.

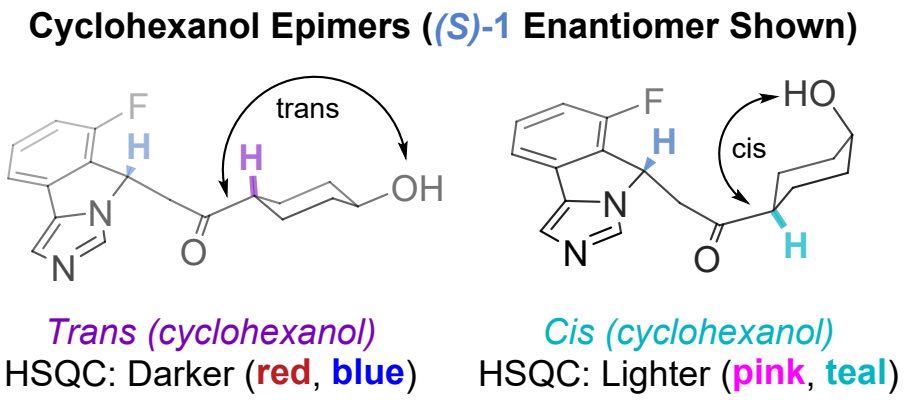

Figure SI 50. Comparison between structures of compound **1** (left, trans cyclohexanol) and compound **3** (right, cis cyclohexanol) for the (*S*)-enantiomers, illustrating proposed configurational differences leading to the shifted resonances observed in Figure SI 49.

12. References

1. A. J. Kukor, M. A. Guy, J. M. Hawkins, J. E. Hein, *React. Chem. Eng.* **2021**, *6*, 2042–2049.
2. F. St-Jean, R. Angelaud, S. Bachmann, D. E. Carrera, T. Remarchuk, K. A. Piechowicz, K. Niedermann, H. Iding, R. Meier, H. Hou, L. E. Sirois, J. Xue, M. Olbrich, P. Rege, M. Guillemot-Plass and F. Gosselin, *J. Org. Chem.,* **2022**, *87*, 4955−4960.
3. A. Cote, D. Erdemir, K. P. Girard, D. A. Green, M. A. Lovette, E. Sirota and N. K. Nere, Cryst. Growth Des., 2020, *20*, 7568–7581.
4. L. H. Nicoud, A. S. Myerson, The Influence of Impurities and Additives on Crystallization. In *The Handbook of Industrial Crystallization*, 3rd ed.; A. S. Myerson, D. Erdemir, A. Lee, Eds.; Cambridge University Press: Cambridge, U.K., **2019**; 115−135.
5. M. Wernerova, T. Hudlicky, On the Practical Limits of Determining Isolated Product Yields and Ratios of Stereoisomers: Reflections, Analysis, and Redemption. *Synlett* **2010**, *18*, 2701–2707.